

FUSE OBSERVATIONS OF THE MAGELLANIC BRIDGE GAS TOWARD TWO EARLY-TYPE STARS: MOLECULES, PHYSICAL CONDITIONS, AND RELATIVE ABUNDANCES

N. LEHNER

The Johns Hopkins University, Department of Physics and Astronomy, Bloomberg Center, 3400 N. Charles Street, Baltimore, MD 21218 (nl@pha.jhu.edu)

Draft version June 27, 2021

ABSTRACT

We discuss *Far Ultraviolet Spectroscopic Explorer* (*FUSE*) observations of two early-type stars, DI 1388 ($l = 291.3^\circ$, $b = -41.1^\circ$) and DGIK 975 ($l = 287.3^\circ$, $b = -36.0^\circ$), in the low density and low metallicity ($Z \sim 0.08Z_\odot$) gas of Magellanic Bridge (MB). The data have a spectral resolution of about 15,000 and signal-to-noise ratios range between 10 and 30 per resolution element in the spectra of DI 1388 and between 7 and 11 in the spectra of DGIK 975. DI 1388 is situated near the SMC, while DGIK 975 is closer to the LMC, allowing us to probe the MB gas in a widely different locations. Toward DI 1388, the *FUSE* observations show molecular hydrogen, O VI, and numerous other atomic or ionic transitions in absorption, implying the presence of multiple gas phases in a complex arrangement. The relative abundance (with respect to S II) pattern in the MB along the DI 1388 sight line is attributed to varying degrees of depletion onto dust similar to that of halo clouds. The N/O ratio is near solar, much higher than N/O in damped Ly α systems, implying subsequent stellar processing to explain the origin of nitrogen in the MB. The diffuse molecular cloud in this direction has a low column density and low molecular fraction ($\log N(\text{H}_2) \approx 15.43$ dex; $f_{\text{H}_2} \sim 10^{-5} - 10^{-4}$), yet two excitation temperatures ($T_{01} = 94 \pm {}_{27}^{53}$ K and $T_{23} = 341 \pm {}_{81}^{172}$ K) are needed to fit the distribution of the different rotational levels. Though this is not typically seen in the Galaxy, we show that this is not uncommon in the Magellanic Clouds. H_2 is observed in both the Magellanic Stream and the MB, yet massive stars form only in the MB, implying significantly different physical processes between them. In the MB some of the H_2 could have been pulled out from the SMC via tidal interaction, but some also could have formed *in situ* in dense clouds where star formation might have taken place. Toward DGIK 975, the presence of neutral, weakly and highly ionized species suggest that this sight line has also several complex gas phases. The highly ionized species of O VI, C IV, and Si IV toward both stars have very broad features, indicating that multiple components of hot gas at different velocities are present. C IV/O VI varies within the MB but C IV/Si IV is relatively constant for both sight lines. Several sources (a combination of turbulent mixing layer, conductive heating, and cooling flows) may be contributing to the production of the highly ionized gas in the MB. Finally, this study has confirmed previous results that the high-velocity cloud HVC 291.5 – 41.2 + 80 is mainly ionized composed of weakly and highly ions. The high ion ratios are consistent with a radiatively cooling gas in a fountain flow model.

Subject headings: Galaxies: abundances — ISM: abundances — Magellanic Bridge — ISM: structure

1. INTRODUCTION

The Magellanic system is composed of two small irregular galaxies, the Large (LMC) and Small (SMC) Magellanic Clouds, in orbit around the Galaxy. Tidal interactions between these galaxies have produced several high velocity gas complexes connected to the Clouds (for a recent study, see Putman 2000); namely the Magellanic Bridge (MB), the Magellanic Stream, and the leading Arm. In particular for this study, the Magellanic Bridge is a 10° region of tenuous gas linking the body of the SMC to an extended arm of the LMC. The formation mechanism responsible for this feature remains unclear, but it is generally agreed that the MB was formed via a tidal encounter between the SMC and LMC. Gardiner & Noguchi (1996) have produced models that can reproduce simultaneously both the MB and the Magellanic Stream, and find that the MB was most likely pulled from the wing of the SMC 200 Myr ago during a close encounter between the two Clouds. However, its low metallicity ($Z \approx 0.08Z_\odot$ based on C, N, O, Mg, and Si Rolleston et al. 1999) does not reflect the current SMC metallicity ($Z \approx 0.25Z_\odot$, e.g., Rus-

sell and Dopita 1992), suggesting that the MB gas could be formed from a mixture of SMC gas and an unenriched component or could be much older than the age predicted from theoretical models.

The MB contains early-type stars (Hambly et al. 1994; Demers & Battinelli 1998; Rolleston et al. 1999). During their main-sequence lifetimes (as short as 20 Myr), these stars could not possibly migrate from the SMC since they do not exhibit peculiar velocities sufficient to explain their motion over the large distances they would need to cover. Therefore the MB provides the most metal poor gas in our neighborhood to investigate not only the gas, but also to observationally constrain star-formation in low metal and tenuous gas environment. Furthermore, it provides an unique opportunity to study in detail the gas resulting from tidal interactions. In the Galaxy, star formation generally occurs in dense molecular clouds (e.g., Evans 1999). No direct evidence of molecular clouds have been discovered yet (Smoker et al. 2000), although Kobulnicky & Dickey (1999) found cold atomic clouds, suggesting molecular condensations.

Lehner et al. (2001) recently reported the results of a program to investigate the chemical composition and abundance pattern of the MB gas toward an early-type star, DI 1388, with the *Hubble Space Telescope* (*HST*) and the Space Telescope Imaging Spectrograph (STIS). The combination of high spectral resolution and high sensitivity in the ultraviolet bandpass (1150 – 1730 Å) made it feasible to investigate the chemical composition and the physical conditions within the MB and revealed complex gas phases with neutral gas, weakly and highly ionized gas along the sight line studied. Yet only at lower wavelengths than the STIS bandpass, in the 905–1187 Å wavelength range, are the strong hydrogen molecular lines accessible. Other strong atomic and ionic resonance lines are as well only limited in this bandpass, such as the O VI doublet, a powerful diagnostic of collisionally ionized gas. O VI is unlikely to be produced by photoionization alone from starlight given that photons with $h\nu \geq 114$ eV are needed to convert O V to O VI. Such a bandpass is accessible now with the *Far Ultraviolet Spectroscopic Explorer* (*FUSE*) and therefore follow-up observations of the low metallicity, tenuous gas of the MB were obtained with this observatory.

In this article, we report on *FUSE* observations of two early-type stars in the MB, DI 1388 which is situated approximately mid-way between the SMC and LMC and DGIK 975, which lies at the western end of the Bridge near to the LMC halo. The *FUSE* spectra allow us for the first time to make a sensitive and direct search for molecules in the MB. They provide a means to study the collisional gas seen in O VI absorption and to compare with recent O VI surveys in the SMC and LMC (Hoopes et al. 2002; Howk et al. 2002a) and in the Galactic halo (Savage et al. 2000). They also provide a quantitative estimate of the quantities of neutral and weakly ionized gas in the MB and in the ionized high-velocity cloud HVC 291.5 – 41.2 + 80 (Lehner, Keenan, & Sembach 2001).

2. OBSERVATIONS AND DATA PROCESSING

We obtained *FUSE* spectra of two early-type stars, DI 1388 ($l = 291.3^\circ$, $b = -41.1^\circ$) and DGIK 975 ($l = 287.3^\circ$, $b = -36.0^\circ$), in the MB on 2001 August 15 and August 24, respectively. A summary of their stellar properties and location is given in Table 1. The data are cataloged in the MAST archive under the identifications P2410101 and P2410201. Total exposure times of 17,460 seconds for DI 1388 and 23,520 seconds for DGIK 975 were obtained. All the data were obtained in time-tag mode through the $30'' \times 30''$ aperture.

The *FUSE* instrument consists of four channels: two optimized for the short wavelengths (SiC 1 and SiC 2; 905–1100 Å) and two optimized for longer wavelengths (LiF 1 and LiF 2; 1000–1187 Å). There is, however, overlap between the different channels, and, generally, an atomic or a molecular transition appears in at least two different channels. More complete descriptions of the design and performance of the *FUSE* spectrograph are given by Moos et al. (2000) and Sahnou et al. (2000), respectively. To maintain optimal spectral resolution and information on the fixed-pattern noise, the individual segments were not co-added together. For both sight lines, all the four channels were reasonably co-aligned throughout the observa-

tion, but for DGIK 975, detector 2 was shutdown for most of the observation resulting in the loss of SiC 2 and LiF 2 data (note as well that 3/14 exposures in SiC 1 were lost). Therefore only the LiF 1 channel is used in this work for the DGIK 975 sight line.

Standard processing with the current version of the calibration pipeline software (*CALFUSE* v2.0.5) was used to extract and calibrate the spectra. The software screened the data for valid photon events, removed burst events, corrected for geometrical distortions, spectral motions, satellite orbital motions, and detector background noise, and finally applied flux and wavelength calibrations. The extracted spectra associated with the separate exposures were aligned by cross-correlating the positions of strong interstellar lines, and then co-added. The co-added spectra were rebinned by 4 pixels (~ 27 mÅ) since the extracted data are oversampled. Scattered light and detector backgrounds are negligible at the flux levels of the absorption lines considered in this work. The spectra have a nominal spectral resolution of $\sim 15,000$ (≈ 20 km s $^{-1}$; 2 pixels FWHM). For DI 1388, the spectra have a signal-to-noise (S/N) ratio in the continuum between 10 and 30 per resolution element; and for DGIK 975 between 7 and 12 per resolution element. In Tables 2 and 3, the S/N levels are given for each studied transitions and were determined by examining the dispersion about low-order polynomial fit to the continuum in the vicinity of the specified absorption lines. The relative wavelength calibration is accurate to about ± 5 km s $^{-1}$ but can vary by 10–15 km s $^{-1}$ over small wavelength intervals. The zero point of the wavelength scale was set by comparing absorption at *FUSE* wavelengths to longer UV or optical wavelengths. The MB component is present at $v_{\text{LSR}} \sim 200$ km s $^{-1}$ toward DI 1388, and at $v_{\text{LSR}} \sim 170$ km s $^{-1}$ toward DGIK 975.

We illustrate in Figure 1 the reduced *FUSE* spectra of DI 1388 for different detector segments. The data reveal numerous stellar and interstellar atomic and molecular absorption lines. Interstellar lines are identified when both the Galactic and MB components are present. The H I Lyman-series can be easily identified. Broader features are stellar lines. Because the *FUSE* bandpass is very rich in interstellar lines, a careful check was made to ensure that no other line was blended with the MB component. We note that while the airglow lines are relatively strong (see Figure 1, especially H I and O I), they do not affect the MB measurements as those lines are shifted by $\gtrsim +150$ km s $^{-1}$.

3. ANALYSIS

The stellar continua were simple enough near the interstellar lines in the *FUSE* bandpass to be fitted with low-order (≤ 4) Legendre polynomials. A selection of normalized profiles is shown in Figures 2 and 3 for the DI 1388 and DGIK 975 sight lines, respectively. Species detected in the *FUSE* spectra in absorption are: (1) For DI 1388, C II, C III, N I, N II, N III, O I, O VI, P II, S III, Ar I, Fe II, Fe III, and H₂. ; (2) For DGIK 975, C II, N I, N II, O I, O VI, Si II, Fe II, and Fe III. The absorption lines are stronger toward DGIK 975, and therefore more likely to be saturated. Moreover, the lower S/N of the DGIK 975 spectra hinders precise measurements toward this sight line and also limits the possibility of detecting

weak features.

The equivalent widths were measured by directly integrating the intensity and are listed in Table 2 and 3. The equivalent width measurements and errors were derived following the method described by Sembach & Savage (1992).

To obtain the column density, two methods were used:

(1) The apparent optical depth (AOD) method (Savage & Sembach 1991) was used when only one or two lines of the same atomic species were available. The absorption profiles were converted into apparent optical depths per unit velocity, $\tau_a(v) = \ln[I_c/I_{\text{obs}}(v)]$, where I_c , I_{obs} are the intensity without and with the absorption, respectively. $\tau_a(v)$ is related to the apparent column densities per unit velocity, $N_a(v)$ ($\text{cm}^{-2} (\text{km s}^{-1})^{-1}$) through the relation $N_a(v) = 3.768 \times 10^{14} \tau_a(v) / [f\lambda(\text{\AA})]$. The integrated apparent column density is equivalent to the true integrated column density if no unresolved saturated structure is present. The results are summarized in Tables 2 (DI 1388) and 3 (DGIK 975). The results for the O VI absorption profile and other highly ionized species are discussed in § 4.3 (DI 1388) and § 5 (DGIK 975).

(2) A curve-of-growth (COG) analysis was undertaken when several lines were present (N I, O I, Fe II and H₂ toward DI 1388) by using measured equivalent widths. Additional lines for the atomic species were used from the measurements in the *HST*/STIS spectra (see, Lehner et al. 2001). A single component Gaussian (Maxwellian) curve of growth was constructed in which the Doppler parameter b and the column density were varied to minimize the χ^2 between the observed equivalent widths and a model curve of growth. For DI 1388, the results are summarized in Figures 4 (atomic species) and 5 (H₂). For H₂, a COG was constructed for the lines within each rotational level ($J = 0, \dots, 3$; no detectable absorption is present in levels $J \geq 4$), and this resulted in the COG presented in Figure 5, describing simultaneously all the rotational levels with a Doppler parameter of $b = 2.6 \pm 0.6_{-0.2}^0 \text{ km s}^{-1}$. The $J = 0$ level is poorly constrained as only two transitions were available.

Good agreement is found between the AOD and COG methods for Fe II, principally because the transitions for this ion are not saturated. The transitions of the neutral species lie near or on the knee of the COG where saturation effects arise. The b -values are comparable to the total b -values obtained by Lehner et al. (2001) with the higher spectral resolution of the *HST*/STIS data using a profile fitting method; in particular, the same pattern is observed, i.e. a smaller b -value for N I compared to O I and Fe II, but a similar b -value for O I and Fe II. For DGIK 975, the Fe II column density derived with the COG method is in the range given by the AOD method, but because the lines are much stronger, the S/N is low, and only four transitions are available, the b -value is not constrained. Optical Ca II K spectra of DGIK 975 with similar quality to those described in Lehner et al. (2001) toward DI 1388 (spectral resolution of about 7.1 km s^{-1}) do not show any evidence of multiple component structure. However, Ca II K cannot *a priori* be used to model Fe II component structure in diffuse clouds, as it traces mainly cold neutral clouds, while

Fe II can be found in both neutral and ionized clouds.¹ Note as well that finer structure seen in higher resolution spectra of Galactic HVCs (e.g., Lehner et al. 1999) suggests that the true component structure in the MB gas toward both sight lines may be more complex than is revealed by 6.5 km s^{-1} or lower spectral resolution.

Since we have information on N I and N II toward DI 1388, it is interesting to estimate the amount of interstellar N III. N III $\lambda 989.799$ is severely blended with Si II $\lambda 989.873$. Using the equivalent measurements available in the STIS bandpass for Si II (Lehner et al. 2001), we constructed a COG and estimated the equivalent width for Si II $\lambda 989.873$ as being $\sim 105 \text{ m\AA}$. Knowing the total equivalent width of this feature and assuming that neither lines suffer from saturation effect, we infer that the N III absorption feature has an equivalent width of $\sim 31 \text{ m\AA}$, and with the assumption that it lies on the linear part of the COG, its column density is ~ 13.5 dex.

The 3σ upper limits for the equivalent widths in Table 2 are defined as $W_{\text{min}} = 3\sigma \delta\lambda$, where σ is the inverse of continuum S/N ratio and $\delta\lambda \approx 0.1 \text{ \AA}$, which is approximately the average FWHM obtained from the resolved features. The corresponding 3σ upper limits on the column density are obtained from the corresponding equivalent width limits and the assumption of a linear curve of growth.

We adopted wavelengths and oscillator strengths from the Morton (2000, private communication) atomic data compilation. This compilation is similar to the Morton (1991) compilation with a few minor updates to the atomic parameters for lines of interest in this study. For the Fe II lines, the new oscillator strengths derived by Howk et al. (2000) were adopted. We note that there is a new laboratory measurement of the f -value for Fe II $\lambda 1144.9$ ($f = 0.083 \pm 0.006$, Wiese, Bonvallet, & Lawler 2002), about 30% lower than the experimental value of Howk et al. (2000). We note, however, that the value of Howk et al. gives a column density in good agreement with the measurement from the Fe II $\lambda 1608.4$ line. Moreover, Wiese, Bonvallet, & Lawler (2002) note that additional study is necessary for the other transitions available in the *FUSE* bandpass, rather than a simple rescaling, as they are further down on the COG than the Fe II $\lambda 1144.9$ line. As we use all the transitions available in *FUSE* spectrum, we employ the f -value of Howk et al. (2000) and we note that even if f -values are lower, the column density would only change by about $+0.05$ dex, and our conclusions would remain the same. The H₂ wavelengths are from Abgrall et al. (1993a,b), while the H₂ f -values were calculated from the emission probabilities given by those authors.

4. MAGELLANIC BRIDGE GAS TOWARD DI 1388

4.1. Molecular hydrogen

Until recently, searches for molecular gas in the MB were restricted to observations of CO (Smoker et al. 2000), but none was found, mainly due to a lack of sensitivity. The most abundant molecule in the Universe, molecular hydrogen (H₂) has only been recently accessible with the launch of *FUSE* for faint targets observed in the MB. *FUSE* observations reveal that 92% and 52% of the SMC and LMC sources, respectively, exhibit H₂ absorption lines (Tum-

¹ D.E. Welty (private communication, 2002) has noted, however, that comparisons of high spectral resolution profiles for Ca II and Fe II can show surprising similarity in many cases.

linson et al. 2002). Two observations toward the Magellanic Stream also reveal H₂ (Sembach et al. 2001; Richter et al. 2001). While the S/N is too low in the spectrum of DGIK 975 to allow any conclusions, the spectrum of DI 1388 exhibits about 30 absorption lines from the Lyman and Werner bands of H₂ (see Table 2). In all known environments in our Galaxy, star formation occurs within molecular clouds. The detection of H₂ toward DI 1388 is therefore the first direct evidence of a possible star formation signature in the very poor metal environment of the MB.

From Table 2 and Figure 5, the total column density of H₂ is $\log N(\text{H}_2) \approx 15.43$ dex. For $J \geq 4$, $\log N_J(\text{H}_2) < 14.0$ dex. The H I column density is not well known (Lehner et al. 2001): the H I emission column density is 20.50 dex (Putman 2000, private communication; see Lehner et al. 2001a). In theory, the *FUSE* observations could help to constrain the H I absorption column density because numerous H I lines of the Lyman series with different oscillator strengths are accessible. Moreover, at $\lambda < 926.2$ Å, the MB component can be separated from the lower velocity components. But as displayed in Figure 1, the continuum position is uncertain at these wavelengths. The stellar contribution is also not known due to the difficulty to model this star because its large $v \sin i$. Therefore, the H I absorption column density cannot be directly derived. An alternative is to use the O I column density. O I is an excellent tracer of neutral gas as its ionization potential and charge exchange reactions with hydrogen ensure that the ionization of H I and O I are strongly coupled. Using the O I column density, and assuming the interstellar O abundance² found by Meyer et al. (1998) $\text{O}/\text{H} = (3.43 \pm 0.15) \times 10^{-4}$, and a general deficiency in metal of the MB gas of -1.1 dex from the stellar study (Rolleston et al. 1999), we obtain $\log N(\text{H I}) \approx 19.72$ dex. The difference could be due to the large beam of the H I emission data and to the position (in depth along the sight line) of DI 1388 in the MB.

Using the H I value derived from O I, the fractional abundance of H₂ is $f_{\text{H}_2} \equiv 2N(\text{H}_2)/[N(\text{H I}) + 2N(\text{H}_2)] \sim 1 \times 10^{-4}$, while the H I emission column density suggests $f_{\text{H}_2} > 2 \times 10^{-5}$. This value is comparable to those seen along Galactic sight lines (Savage et al. 1977) and Magellanic Clouds sight lines (Tumlinson et al. 2002) when $E(B-V) \lesssim 0.1$ and $\log[N(\text{H I}) + 2N(\text{H}_2)] \lesssim 20.5$ dex. However, Tumlinson et al. (2002) noted that a major difference between the Galactic and Magellanic Clouds samples is the presence of several sight lines with $f_{\text{H}_2} \gtrsim 10^{-4}$ when $E(B-V) \lesssim 0.08$. We also note that for similar H₂ column densities in the SMC and LMC, molecular fractions similar to that derived here are observed. For the MB, and in some cases for the SMC and LMC (see Figure 12 in the Appendix), f_{H_2} remains uncertain due to H I column density uncertainties.

The population of the lower rotational states of molecular hydrogen is determined by collisional excitation with a Boltzmann distribution, so that the excitation temperature T_{ij} is given by (e.g., Spitzer, Cochran, & Hirshfeld

1974)

$$T_{ij} = \frac{E_j - E_i}{k \ln \left[\frac{g_i N_j}{g_j N_i} \right]}. \quad (1)$$

We find that $T_{01} = 94 \pm {}^{53}_{27}$ K and $T_{23} = 341 \pm {}^{172}_{81}$ K. In Figure 6, the excitation temperature diagram is presented for H₂ arising in ground-state rotational levels $J \leq 4$. The interpretation of this diagram is complicated by the large uncertainty in the column density of the $J = 0$ level. In their survey in the Galaxy, Spitzer, Cochran, & Hirshfeld (1974) found that when $N(J = 0) \lesssim 10^{15}$ cm⁻², a single excitation temperature generally fits all the observed $N(J)$ within their estimated errors. Toward DI 1388 $N(J = 0) \approx 10^{14.88}$ cm⁻², but we believe that the estimated error of this level is conservative and therefore a single temperature does not describe the distribution of the data points within the error bars. In the Appendix, we show by using the LMC and SMC sample that for low H₂ column density, a single excitation temperature does not *generally* fit the distribution of the data points, as observed in the MB, when $N(J = 0) \lesssim 10^{15}$ cm⁻².

The $J = 0, 1$ temperature, though uncertain, is in general agreement with what is derived in diffuse molecular clouds in the Magellanic Clouds ($\langle T_{01} \rangle = 115$ K for all their sight lines; Tumlinson et al. 2002), the Galactic halo ($\langle T_{01} \rangle = 107 \pm 17$ K; Shull et al. 2000), and in the Galactic disk ($\langle T_{01} \rangle = 77 \pm 17$ K; Savage et al. 1977). The absolute value of T_{01} suggests a closer similarity to the Clouds and the Galactic halo than the Galactic disk, yet the large error on T_{01} prevents us from drawing definitive conclusion. While T_{01} may trace directly the kinetic temperature in dense molecular clouds, in low column diffuse clouds the relationship between the excitation temperature of the first two levels and the kinetic temperature is not well understood (e.g.; Tumlinson et al. 2002).

4.2. Neutral and partially ionized gas

Lehner et al. (2001) found two MB interstellar clouds toward DI 1388 at 179 and 198 km s⁻¹ with the 6.5 km s⁻¹ spectral resolution of the *HST*/STIS. The 198 km s⁻¹ cloud is mainly neutral with a hot component (see § 4.3); while the 179 km s⁻¹ cloud is warmer, low density gas, and partially ionized. The *FUSE* bandpass gives access to a large number of ions not accessible with STIS, though at lower resolution, which complicates the interpretation of the data. In particular the separation between the two clouds is about the resolution of *FUSE* and therefore these clouds cannot be resolved with *FUSE*. However, some properties of this sight line can still be derived, since for the neutral and singly ionized species we know from Lehner et al. (2001) that the mainly neutral gas at 198 km s⁻¹ is about 2–3 times stronger in column density than the ionized cloud at 179 km s⁻¹.

The detection of H₂ at ~ 200 km s⁻¹ suggests that it is associated with the neutral cloud observed in the atomic and ionic species. While the excitation temperature T_{01} is relatively low, it is not known how it is related to the kinetic temperature in diffuse clouds. However, the b -value obtained from the COG analysis for H₂ gives an upper limit to the kinetic temperature of $\lesssim 800$ K. We

² Meyer et al.'s value ($\text{O}/\text{H} = (3.19 \pm 0.14) \times 10^{-4}$) was corrected for the recommended oscillator strength of O I $\lambda 1356$ ($f = 1.16 \times 10^{-6}$ instead of $f = 1.25 \times 10^{-6}$) by Welty et al. (1999b).

note that both the COG and profile fitting analysis give a lower b -value for N I compared to O I, suggesting that the mostly neutral cloud is probably composed of more than one cloud. This is also supported by the fact that the profile fitting to O I λ 1302 indicates that some unresolved structures remain (see Figure 2 in Lehner et al. 2001).

For the MB gas we find, when considering the total column density, $N(\text{Fe II})/N(\text{Fe III}) \approx 1.9$, $N(\text{S II})/N(\text{S III}) \approx 4.6$. Sembach et al. (2000) have produced models of low density photoionized gas, and these ratios compare with a combination of their composite and “ $x_{\text{edge}} = 0.95$ ” models. Such models typically simulate regions with significant fraction of neutral hydrogen or ionized interfaces of neutral clouds. Considering only the ionized component for S II and Fe II (see, Lehner et al. 2001) and assuming that S III and Fe III is mostly present in the ionized gas, the ratios are $N(\text{Fe II})/N(\text{Fe III}) \approx 0.5$, $N(\text{S II})/N(\text{S III}) \approx 1.2$. In this situation, the S II/S III ratio is comparable to a low density H II region with a ionization parameter $\log q = -4$ ($\log q \gtrsim -1$ for typical bright high density H II regions, Sembach et al. 2000) and “ $x_{\text{edge}} = 0.10$ ” (i.e. fully ionized material); while Fe II/Fe III is, for a low density H II region, a combination of “ $x_{\text{edge}} = 0.10$ ” and “ $x_{\text{edge}} = 0.95$ ” with $\log q = -4$. Because the ionization potential of Fe III is 16.18 eV smaller than the ionization potential of S III, 23.33 eV, this suggests that a fraction of Fe III could remain in the neutral gas, while S III is mostly in the ionized cloud. We note that the Sembach et al.’s models were simulated with Galactic abundances. Metallicity effects should be negligible on ionization fractions, as long as the relative abundances are similar (see § 4.4).

The determination that $N(\text{N I})/N(\text{N II}) \lesssim 1.0$ shows that N has a deficiency of its neutral form. Because Ar (and N) is not significantly depleted onto dust grain (Sofia & Jenkins 1998), the large deficiency of Ar I in the MB (see Table 7) is certainly due to photoionization. Ar is more easily photoionized than H because its photoionization cross section is about 10 times that of H. N I has a photoionization cross section larger than that of H I and a charge-exchange rate coefficient for N II with H I only twice the recombination coefficient, so that N may show a deficiency of its neutral form, similar to what is observed for Ar (Jenkins et al. 2000a). We note also that N II is the dominant ion along this sight line as $N(\text{N III})/N(\text{N II}) \lesssim 0.2$. Because the b -values for N I and H₂ are similar, it could be that N I, H₂, and the remaining Ar I are in the colder part of the cloud, while some of O I is partly in the cold part but as well in another mostly neutral layer of gas, where sufficiently energetic photons have ionized N and Ar (assuming the different layers/clouds are spatially related).

4.3. Highly ionized species

Lehner et al. (2001) found Si IV and C IV interstellar absorptions in the spectrum of DI 1388. O VI is the most important ion for the study of hot gas and in particular the ratio of C IV/O VI is an important key to differentiate between different theoretical models. O VI is difficult

to produce through photoionization, since it requires photons with energy greater than 114 eV, and is therefore most likely collisionally ionized. It peaks in abundance at 3×10^5 K, compared to 2×10^5 K, 1×10^5 K, and 6×10^4 K for N V, C IV, and Si IV, respectively. O VI is either produced via cooling from higher temperatures or from heating. Several models have been proposed to account for O VI in the ISM, including shock heating, conductive heating, radiative cooling, and turbulent mixing layers (TMLs) (Shull & McKee 1979; Borkowski, Balbus, & Fristrom 1990; Slavin, Shull, & Begelman 1993; Spitzer 1996, and references therein for a summary). These models make different predictions for the various ratios of the highly ionized species, in particular, for convective heating $0.1 \lesssim N(\text{C IV})/N(\text{O VI}) \lesssim 0.3$, for radiative cooling, $0.1 \lesssim N(\text{C IV})/N(\text{O VI}) \lesssim 0.5$, and for TMLs, $N(\text{C IV})/N(\text{O VI}) \gtrsim 1$ (Spitzer 1996; Sembach et al. 2001, and references therein).

As seen in Figure 10, the O VI absorption profile toward the DI 1388 sight line is strong for the Galactic gas between -50 and 50 km s^{-1} and becomes weaker at positive velocity up to $\sim 250 \text{ km s}^{-1}$. There is therefore no clear separation between the Galactic disk/halo and MB components. We note also that some of the observed O VI absorption could have a stellar-wind origin (Lehner et al. 2001c), yet the interstellar O VI origin seems more plausible as wind features typically have full-width larger than few hundreds km s^{-1} . Moreover, O VI absorption profiles toward the Magellanic Clouds are generally very broad with the Galactic and LMC/SMC components being blended (Howk et al. 2002a; Hoopes et al. 2002). In Figure 7, we compare the absorption profiles of the highly ionized species observed in the FUSE (O VI) and STIS (C IV and Si IV, see also Lehner et al. 2001) bandpass. The local component ($[-50, 50] \text{ km s}^{-1}$) is strong and well defined for all the highly ionized species. But at higher positive velocities, C IV and Si IV have a strong absorption MB component ($[155, 245] \text{ km s}^{-1}$) while O VI is relatively weak, whereas at velocities $\lesssim 155 \text{ km s}^{-1}$, the O VI profile becomes deeper. The difference in the profiles of C IV and Si IV with respect to O VI at $\sim 200 \text{ km s}^{-1}$ could be due to that some of the C IV and Si IV originated from photoionization.

As O VI, C IV, and Si IV are usually related, in view of the broad extent of the O VI profile, we decided to redo the analysis of C IV and Si IV by considering different possible continua. This is shown in Figure 7, where the deep Gaussian and polynomial continua fit a stellar line that goes to the bottom of the absorption profiles. Shallower stellar profiles also seem possible to allow the interstellar C IV and Si IV to be present at all velocities as observed for O VI. The resulting column density measurements are summarized in Table 4 for different velocity intervals.³ The errors presented in this Table were obtained following the method outlined by Sembach & Savage (1992). The differences between the various measurements reflect systematic differences that result from various choices for the wavelength intervals or methods defining the (unknown)

³ Lehner et al. (2001) used only a Gaussian fitting method but they also allow possible renormalization of the profiles. For Si IV we find similar results, while C IV is slightly lower, though in agreement within the uncertainties. However, their main result was from the direct comparison of apparent column density profiles of C IV and Si IV. Their derived $N(\text{C IV})/N(\text{Si IV})$ ratio gives a similar C IV column density, assuming their Si IV column density.

location of the true continuum. Note that the C IV $\lambda 1548$ is at the edge of the échelle order and only the MB component could be (partially) retrieved; column densities for the C IV doublet are in good agreement. The Si IV doublet gives very similar results. However, saturation effects are difficult to estimate due to the uncertainty in the continuum placements.

In Table 5, we present the adopted column densities and column density ratios of the highly ionized species. For C IV and Si IV and for all the column density ratios, the error bars indicate the range of possible values rather than a 1σ uncertainty, yet the upper error could be larger if the stellar line is even shallower. We did not take into account the high continuum for C IV $\lambda 1550$ in these adopted results, but this does not change the main conclusions (see below).

The TML model best reproduces the observed ratios of C IV to O VI and Si IV for the main MB component between 155 and 245 km s^{-1} . If C IV and Si IV column densities are underestimated, the agreement with the TML model would be strengthened, since it requires $N(\text{C IV})/N(\text{O VI}) \gtrsim 1$. The different gas phases observed at close or indistinguishable velocities also give some evidence for such a model because cold gas, partially ionized gas and hot gas phases are encountered along this sight line (see Figure 1 in Slavin, Shull, & Begelman 1993). These models usually assume solar abundances or Galactic depletion and it would be interesting to investigate in more details the effect of low metallicity as observed in the MB. We note, however, that neither the stellar abundances from a few early-type stars (Rolleston et al. 1999) nor the relative ISM abundances along this sight line show any anomalies in the relative abundance of the metals. For lower MB velocities (100–155 km s^{-1}), the ratios are very uncertain due to the continuum placement, but suggest a combination of TML and conductive interfaces. The HVC component is very uncertain (see § 6). The ratios of highly ionized species for the strong local component is in agreement to what is found in the Galactic disk and halo; and the radiatively cooling fountain provides a reasonable description of the observed ratios toward DI 1388 (see, Sembach, Savage, & Hurwitz 1999; Spitzer 1996, and references therein).

The amount of H II can be roughly estimated along this sight line from the O VI measurement via $N(\text{H II}) = N(\text{O VI})(\text{O}/\text{H})_{\text{MW}}^{-1} Z^{-1} f_{\text{O VI}}^{-1}$. Assuming an O VI ionization fraction $f_{\text{O VI}} \leq 0.2$ (Tripp & Savage 2000), a present-day metallicity $Z = 0.08 Z_{\odot}$ (Rolleston et al. 1999), and a Galactic interstellar abundance $\text{O}/\text{H} = (3.43 \pm 0.15) \times 10^{-4}$ (see § 4.1), $\log N(\text{H II}) \approx 18.40$ dex in the range [155, 245] km s^{-1} and $\log N(\text{H II}) \approx 18.85$ dex in the range [100, 245] km s^{-1} , implying that neutral gas dominates along this sight line.

4.4. Depletion of the gas

In the Galactic interstellar gas, the underabundances of elements along various sight lines are usually attributed to the depletion of these elements into dust. The nucleosynthetic history of the gas can also play a role, especially in a low metallicity and tidally disrupted gas. Yet, toward DI 1388, Lehner et al. (2001) showed that the principal factor for deficiency of heavy elements is certainly deple-

tion onto dust grains. Here, we combine *FUSE* and STIS results to develop more insight into the depletion and possible ionization correction. Since S II is only modestly depleted in the Galactic ISM, we used it as the reference ion. We compared the elements using the logarithmic normalized gas-phase abundance,

$$\left[\frac{X^{i+}}{\text{S}} \right] = \log \left(\frac{X^{i+}}{\text{S}^+} \right) - \log \left(\frac{X}{\text{S}} \right)_c, \quad (2)$$

where X^i is the ion under consideration, and $(X/\text{S})_c$ is the ratio for cosmic abundances and X/S is used for $N(X)/N(\text{S})$. Equation 2 assumes that the ion X^{i+} is the dominant form of element X . Since $N(\text{S II})/N(\text{S III}) \sim 4.6$, S II is the dominant form of S. Figure 8 (see also Table 7) shows the comparison in abundance pattern between the different Galactic environments and the results for the MB toward DI 1388, with both the *FUSE* and STIS data. The O I column density is now better constrained compared to the study of Lehner et al. (2001), and the differences observed with the Galactic environment could be mainly due to some ionization effect. Similarly, N I is still very deficient; yet taking into account the ionized component (N II and N III), the depletion of N (> -0.4 dex) is roughly similar to the Galactic environment. The tentative measurement of P II (at worst it should be an upper limit) also suggests a halo-like depletion for the MB. Therefore, it seems that the dominant factor describing the MB gas-phase abundance pattern toward DI 1388 appears to be primary depletion of the elements into dust and secondary ionization for neutral species (O I, N I, and Ar I) rather than nucleosynthetic history, and the depletion pattern follows the pattern seen in the Galactic halo.

5. DGIK 975 SIGHT LINE AND COMPARISON WITH DI 1388 SIGHT LINE

5.1. Weakly ionized species

The data toward DGIK 975 are much less reliable, yet several species were detected: C II, N I, N II, O I, O VI, Si II, Fe II, and Fe III. This list hints that as for the DI 1388 sight line, this sight line has different gas phases, with species dominant in neutral gas (N I, O I), some signatures of weakly ionized gas (N II, Fe III) or highly ionized gas (O VI). Comparisons of the profile in Figure 3 suggest that, as toward DI 1388, several clouds are present along the sight line because N I is mainly observed at ~ 170 km s^{-1} , while for the other species, at lower velocities, one or several clouds are suggested.

The Fe II column densities are consistent with each other within the errors. However, the data have low S/N levels, a resolution of ~ 20 km s^{-1} and the lines are very strong, which might suggest some saturation effect.

5.2. Highly ionized species

HST/STIS observations were obtained toward DGIK 975 (in the same program as the observations of DI 1388) but the data were of too low S/N ratio ($\lesssim 5$ for most of the échelle orders) for a detailed analysis (Lehner 2000). However, since strong O VI absorption is observed, it is interesting to try to estimate the amount of C IV and Si IV along this sight line. C IV and Si IV are much broader than the neutral or weakly ionized species, and we can therefore rebin the STIS E140M data by 3 to about

the *FUSE* spectral resolution in order to improve the S/N without losing too much information. Once rebinned, the *HST* data typically have a S/N of about 10–12. In Figure 9, we present the different absorption profiles for O VI, C IV, and Si IV with the chosen continua. Result of measurements is presented in Table 6. We assumed that there is no contribution from the stellar photosphere. However, the projected rotational velocity ($v \sin i \sim 80 \text{ km s}^{-1}$) is relatively low and the radial velocity is $v_{\text{LSR}} \sim 210 \text{ km s}^{-1}$ so that some of the stellar and interstellar lines could be blended. In this case, the $N(\text{C IV})/N(\text{O VI})$ and $N(\text{Si IV})/N(\text{O VI})$ ratio presented in Table 6 should be considered as an upper limit.

In Figure 11, the O VI apparent column density profiles for DI 1388 and DGIK 975 are compared. Toward DI 1388 there is no clear separation between MB and Galactic disk-halo gas. The dashed line in Figure 11 shows a Gaussian fit to the profile of O VI toward DGIK 975 with FWHM of $83 \pm 15 \text{ km s}^{-1}$, implying a temperature of about $2 \times 10^6 \text{ K}$ if the width of the line is due to thermal broadening alone. For C IV and Si IV, the Gaussian FWHMs are ~ 52 and 35 km s^{-1} , respectively, corresponding to a temperature of $\sim 7 \times 10^5 \text{ K}$. In collisional ionization equilibrium the O VI, C IV, and Si IV peak in abundance at lower temperatures (see § 4.3), so if most of the gas is at this temperature, either large turbulent (non-thermal) motions or multiple components are required to explain these line broadenings. Because the column density is weaker toward DI 1388, we can not fit reliably the O VI line, but its large extent also suggests a large temperature. For C IV and Si IV, the continuum placement is uncertain but suggest a temperature $\gtrsim 2 \times 10^5 \text{ K}$. Both the LMC and SMC surveys of O VI absorption showed similar broad lines (Howk et al. 2002a; Hoopes et al. 2002).

While the amount O VI can not be directly compared in the MB because the location in depth of the stars is unknown, $N(\text{C IV})/N(\text{Si IV})$ is similar for both sight lines, but $N(\text{C IV})/N(\text{O VI})$ (and $N(\text{Si IV})/N(\text{O VI})$) is disparate. This holds even if there is stellar contamination, since toward DI 1388 the $N(\text{C IV})/N(\text{O VI})$ and $N(\text{Si IV})/N(\text{O VI})$ ratios would be lower limits, while toward DGIK 975, they would be upper limits. This suggests variation of the O VI column density across the MB. In contrast, even if the Galactic component of hot gas varies by a factor 2.4 between these sightlines (confirming the recent results of Howk et al. 2002b), the ratio of the highly ionized species agrees roughly within the uncertainties, suggesting that similar mechanisms for the production of highly ionized ions occur toward both sight lines in the Galactic gas.

Comparing with the theoretical models (see § 4.3) toward DGIK 975, a radiatively cooling flow or a combination in the right proportion of TMLs and conductive interface describes the derived ratios reasonably well for the MB component.

6. THE HIGH-VELOCITY CLOUD HVC 291.5 – 41.2 + 80

Using the ultraviolet STIS spectrum of DI 1388, Lehner, Keenan, & Sembach (2001) detected an HVC at $v_{\text{LSR}} \sim +80 \text{ km s}^{-1}$, as well as two very low-column HVCs at $\sim +113$ and $+130 \text{ km s}^{-1}$. The O I and N I deficiencies with respect to C II and the presence of ionized elements

(S III and Si III) indicated that HVC 291.5 – 41.2 + 80 consists of a warm, mainly ionized medium at high Galactic latitude.

In the *FUSE* bandpass, this HVC is detected in absorption via N II and O VI, and their normalized profiles are shown in Figure 10. No Fe III is detected but this is not surprising as the Fe III stellar line is strong and the interstellar HVC component is lost in it. The apparent column density of N II is $13.44 \pm 0.12 \text{ dex}$, confirming that this HVC is largely ionized ($\log N(\text{N I}) < 12.4 \text{ dex}$, Lehner, Keenan, & Sembach 2001). No N III is detected, and we estimated a 3σ upper limit of $< 13.5 \text{ dex}$.

As discussed in § 4.3, there is no clear separation between the different components in the O VI absorption profile (see Figures 10 and 11). We used N II to determine the velocity range ($70\text{--}100 \text{ km s}^{-1}$) over which the O VI intensity profile is integrated. In Table 5, we summarize this measurement along with the results on C IV and Si IV. The latter remains uncertain due to continuum placement (see § 4.3). The C IV/O VI ratio is in agreement with values found in the Galactic disk and near the low end value for the Galactic halo (Spitzer 1996). Zsargó et al. (2002) presented a more recent survey in the low Galactic halo, where they found $N(\text{C IV})/N(\text{O VI}) < 1$ for most sight lines with Galactic height $z \lesssim 4 \text{ kpc}$.

The high ion ratios are consistent with the expectations of a radiatively cooling gas in a fountain flow (Spitzer 1996; Sembach, Savage, & Hurwitz 1999). In a such model hot gas is produced by the cumulative effects of supernovae in the Galactic disk. It provides an explanation for the origin of HVCs in the low Galactic halo with positive velocity (Wakker & van Woerden 1997, and references therein), such as HVC 291.5 – 41.2 + 80. The location of the HVC in the lower part of the halo also provides an explanation of why the gas is mainly ionized, since a sufficient number of photons could leak out of the Galactic disk to cause its ionization. Alternative scenarios are possible but would require the combination of conductive interfaces and turbulent mixing layers.

We note also a tentative detection of an HVC at $\sim +70 \text{ km s}^{-1}$ toward DGIK 975 in the high ions (see Fig. 9). The S/N levels are too low to make any measurements but would confirm that such highly ionized clouds are common.

7. DISCUSSION

7.1. Molecules and star formation in the Magellanic Bridge

Demers & Battinelli (1998) found using deep *BV* CCD photometry that the stars in form of stellar clusters in the MB were formed some 10 to 25 Myr ago. Spectroscopic studies of some of these stars confirm that they are massive young stars but with a metallicity $Z \approx 0.08Z_{\odot}$ (Rolleston et al. 1999), a factor ~ 3 lower than the present day metallicity of the SMC. Their location in the MB also rejects the idea that these stars could be runaway stars from the SMC since they could not travel such large distances over their short life-times. It is generally accepted that the MB was most likely pulled from the wing of the SMC some 200 Myr ago, during a close encounter between the two Clouds, whereas the Magellanic Stream was created by a SMC-LMC-Galaxy close encounter $\sim 1.5 \text{ Gyr}$ ago (Gardiner & Noguchi 1996). Searches for stars in

the Stream have, however, produced largely negative results (see Irwin, Demers, & Kunkel 1990, and references therein). Interstellar study toward two sight lines in the Stream indicates an abundance similar to the abundance in the SMC, $Z \approx 0.25Z_{\odot}$ (Lu et al. 1998; Sembach et al. 2001; Gibson et al. 2000). Yet, because the present-day MB abundance is a factor ~ 3 lower than the present day metallicity of the SMC, Rolleston et al. (1999) postulated that the MB was formed either much earlier (~ 8.5 Gyr ago) from more primordial gas, or some 0.2 Gyr ago from a mixture of SMC gas and an unenriched (primordial) component. Toward both the Magellanic Stream and Bridge, molecules were found, yet because star formation occurs in the MB and not in the Stream, the physical conditions must be different. Even though young stellar clusters exist in the MB (Demers & Battinelli 1998), their formation is not very efficient and only happens in recent times, since the MB gas is poor in metals. Christodoulou, Tohline, & Keenan (1997) suggested that the MB was formed earlier than the Stream, in order to explain why star formation occurs only in the MB. In such a scenario, the low metallicity is explained by the tidal stripping of gas from SMC in its earlier chemical evolution, and stars form late, only after tidally induced cloud mergers have had a chance to occur in substantial numbers, and to produce some massive clouds. Such scenario is supported by some recent H I Parkes All Sky Survey (HIPASS) data of the entire Magellanic Stream which indicate dual filaments that are likely to be relics from gas stripped from the SMC and the MB (Putman et al. 2002). These observations imply that at least some part of the Stream could be younger than the MB, and that the MB could be older than usually assumed (see, Putman et al. 2002). Pairing of galaxies are very common (Barnes & Hernquist 1992), and the SMC and LMC could have been paired since the beginning of their existence, and therefore some part of the MB, if not all, could be much older than previously thought.

The discovery of molecular hydrogen in the MB implies that it is formed *in situ* and/or was tidally stripped from the SMC. Formation of H_2 is thought to occur on interstellar dust grains when hydrogen atoms are adsorbed onto the grain surface and react. An hydrogen molecule is then ejected in the gas phase (e.g., Hollenbach, Werner, & Salpeter 1971). Therefore the formation mechanism is related to the quantity, type of grains, gas density, and metallicity. Dissociation of H_2 depends on the intensity of the ultraviolet radiation field, the presence of hot gas, and the possible effect of shocks. Grains serve as catalysts for the formation of H_2 but also as shields against the ultraviolet radiation. Tumlinson et al. (2002) found that for the LMC and SMC low metallicity gas differences in the formation and destruction balance of H_2 : grain formation rates about 1/3 to 1/10 of the Galactic value and ultraviolet radiation field 10 to 100 times the Galactic mean value. The H_2 formation can be written as $t = 1/(Rn_H)$ (e.g., Shull & Beckwith 1982), where R is the formation rate coefficient, ($R = 1 - 3 \times 10^{-17} \text{ cm}^3 \text{ s}^{-1}$ for Galactic conditions, $R \approx 0.3 \times 10^{-17} \text{ cm}^3 \text{ s}^{-1}$ for LMC, SMC conditions) and n_H the hydrogen column density. Assuming LMC, SMC conditions for the MB, $t = 11/n_H$ Gyr. Along the DI 1388 sight line, n_H cannot be high enough to lower t to the believed 200 Myr year old of the MB, and

therefore from those assumptions most of the observed H_2 has survived the tidal stripping; unless if the MB is much older.

Alternatively, H_2 could have (partially) formed in small compact and dense cloudlets within the MB. Formation of clusters of massive stars occurs in the MB (Rolleston et al. 1999; Demers & Battinelli 1998, and references therein), and if the formation processes are similar to that observed in the Galaxy, this requires very high density clouds and cloud-cloud collisions (Scoville, Sanders, & Clemens 1986; Evans 1999). In this picture H_2 can form rapidly in dense regions and disperse in more diffuse clouds. Therefore the observed diffuse molecular clouds along the DI 1388 sight line could trace or be the remnant of denser molecular clouds, the latter being the place where star formation occurred. The detection of cold H I cloud with spin temperatures between 20 and 50 K in the MB by Kobulnicky & Dickey (1999) also supports the idea that some regions must be at high densities ($\gtrsim 100 \text{ cm}^{-3}$). The pressure in the MB must be low on average, yet tidal interactions between the SMC and LMC could have created strong enough perturbations in the overall low density MB gas to produce high density peaks, conditions not existing in the Stream because possibly the interaction in the MB involves closer galaxies and/or is over a longer time.

7.2. N/O ratio in the Magellanic Bridge

The nucleosynthetic origin of N has been subject of large debate, but its understanding is fundamental for comprehending the chemical evolution of galaxies (Vila-Costa & Edmunds 1993; Henry & Worthey 1999). Nitrogen is mainly produced in the six steps of the CN branch of the CNO bi-cycle within H burning stellar zones, where ^{12}C serves as a catalyst. First generation stars produce their own C during the He burning phase, and N production must be fairly independent of the initial composition of the star of which it is synthesized, and the synthesis is said *primary*. Beyond the first generation of stars, the gas from which these stars formed is already polluted with C and O. The amount of N in this material will be proportional of its C abundance, and the N synthesis is said to be *secondary* in this case. Thus, primary nitrogen is independent of the metallicity, and secondary nitrogen increases with increasing metallicity. Most measurements of N/O in our Galaxy and nearby Galaxies are made in stars and H II regions and only few direct measurements in the gas are available in absorption, and therefore our measurement in the MB is particularly notable.

Toward DI 1388, the MB N/O ratio is $[N/O] = -0.05 \pm 0.02$ (from N I and O I column densities), i.e. near a solar value. Lehner et al. (2001) suggested that N might be deficient in the MB, however, they also noted that this could be mainly due to photoionization effect. The *FUSE* data allow us to have precise measurements of N I and O I but also give access to ionized N via N II and N III. If N I is preferentially ionized with respect to O I, $[N/O]$ would be solar or even above solar. The N/O ratio in the gas is in agreement with the results on the photospheric abundances of the B-type stars analysis where $[N/O] \approx -0.08$ (from a differential abundance analysis, Rolleston et al. 1999). In contrast, in both the LMC and SMC, N in the H II regions is systematically underabundant by a factor

4–6 compared to the main sequence B-type stars (see, Garnett 1999). An analysis of the *FUSE* data using absorption lines could help to constrain N/O in the ISM of the LMC and SMC, and therefore help to comprehend these differences.

Henry, Edmunds, & Köppen (2000) compiled a survey of Galactic and extragalactic H II regions and stars to analyse the behavior of N/O as a function of O/H. They observe a plateau (though with some scatter) of N/O measurements when $[O/H] < -1$ suggesting independence of N/O with metallicity, consistent with primary nitrogen formation; and when $[O/H] \gtrsim -1$, a rise with a large scatter of N/O with metallicity is observed, more suggestive of secondary nitrogen formation. The MB metallicity (-1.1 ± 0.1 dex for C, N, O, Mg, and Si in the photosphere of main sequence B-type stars, Rolleston et al. 1999) is at this apparent boundary. Henry, Edmunds, & Köppen (2000) found, at the MB metallicity, N/O lower by a factor 3 to 10 compared to the MB. Yet, the typical error bars for these measurements are large, typically $\sim \pm 0.4$ dex for $\log(N/O)$ and $\sim \pm 0.2$ dex for $\log(O/H)$, and within the error bars few measurements of N/O in H II regions could have a solar value for a MB metallicity. In the damped Ly α systems, at MB metallicity (or slightly higher or much lower than the MB metallicity), N/O is always at least a factor 3 lower than solar (Prochaska et al. 2002; Lu, Sargent, & Barlow 1998).

From both the studies of the gas and the massive stars, N/O is much higher in the MB than N/O values in the damped Ly α systems, implying that N in the MB is more secondary than primary. Most of nitrogen is formed in intermediate mass-stars ($1-8 M_{\odot}$) with roughly a characteristic lag time of 250 Myr (Henry, Edmunds, & Köppen 2000). If the MB is 200 Myr old (see § 7.1), most of the nitrogen must have come from an N-enriched region of the SMC. Henry, Edmunds, & Köppen (2000) argue that since the distribution of N/O at a single O/H value appears to be clustered toward low N/O values, the high values of N/O might be due to nitrogen enrichment by Wolf-Rayet stars or luminous blue variables.

8. SUMMARY

We have presented *FUSE* observations of two early-type stars (DI 1388 and DGIK 975) in the low density and low metallicity gas of the MB. DI 1388 is situated near the SMC, while DGIK 975 lies near the LMC. Galactic ($v_{LSR} \sim 0 \text{ km s}^{-1}$), HVC ($v_{LSR} \sim 80 \text{ km s}^{-1}$), and MB ($v_{LSR} \sim 150-200 \text{ km s}^{-1}$) components are observed in absorption. The *FUSE* spectra reveal that the MB gas shows a complex arrangement of gas in different phases, including the detection of molecules, neutral, weakly and highly ionized species as observed in the interstellar medium of the Galaxy.

Toward DI 1388, the *FUSE* observations provide detections of molecular hydrogen and O VI. Numerous transitions of the same species available in the *FUSE* bandpass allow us to derive precise column density for O I, N I, and Fe II. It gives also useful information on the amount of N II, N III, Ar I, P II, S III, and Fe III. Combining the previous STIS results (Lehner et al. 2001) with the present results show that the relative abundance pattern with respect to S in the MB along the DI 1388 sight line can be

attributed to varying degrees of depletion onto dust similar to that in halo clouds, despite an overall metallicity much lower, and the depletion pattern follows the pattern observed in the Galactic halo. For N I (and Ar I) the deficiency can be explained by ionization effects, and the amount of N II is at least as large as the amount of N I.

The N/O ratio in the MB toward DI 1388 is near solar, in agreement with the abundance exhibited by early-type stars (see, Rolleston et al. 1999). This is a factor 3 or higher than the values of N/O in the damped Ly α systems, implying subsequent stellar processing (possibly from Wolf-Rayet stars or luminous blue variables) to explain this high N/O ratio for an overall low metallicity.

The diffuse molecular cloud has a low column density ($\log N(H_2) \approx 15.43$ dex), yet two excitation temperatures are needed to fit the distribution of the different rotational levels. We show that this is not uncommon in the Clouds (see Appendix). The low b -value for H $_2$ is similar to the value for N I, whereas O I and other species have larger b -values, implying that several clouds are present along the DI 1388 sight line, including, cold and warm neutral clouds, a partially weakly ionized cloud, and highly ionized cloud.

Toward DGIK 975, the situation is less clear due to lower quality data and stronger lines (more subject to saturation effect). Yet the presence of neutral, weakly and highly ionized species suggest that this sight line has also several gas phases as observed toward DI 1388 or the interstellar gas in the Galaxy.

For the highly ionized species along the sight line to DGIK 975, for the MB component, very broad features of O VI, C IV, and Si IV are observed, indicating that either non-thermal motions are prevalent, or that multiple components of hot gas at different velocities are present. Toward DI 1388, the profile in O VI is extended, but where the O VI absorption is the weakest (main component of the neutral gas at 198 km s^{-1}) C IV and Si IV are the strongest (though some uncertainties remain due to continuum placement), which indicates that C IV and Si IV could have partially originated from photoionization. Similar large broadening were found in LMC and SMC (Howk et al. 2002a; Hoopes et al. 2002). Toward DI 1388, a high ratio of C IV/O VI (> 1) is found for the main component at 198 km s^{-1} that could have originated in a turbulent mixing layer. Toward the SMC star Sk 108, a similar high ratio was found (Mallouris et al. 2001). When considering the more extended absorption profiles toward DI 1388 (in the range $[100, 245] \text{ km s}^{-1}$) the C IV/O VI ratio is lower and more similar to the ratio toward DGIK 975. C IV/O VI varies within the MB but the C IV/Si IV is relatively constant (in comparison) for both sight lines. Several sources (a combination of turbulent mixing layer, conductive heating, and cooling flow) may cause the hot ionized gas in the MB.

H $_2$ is observed in both the Magellanic Stream and the MB, yet the formation of massive stars occurs only in the MB, implying significantly different physical conditions between them. In the MB, some of the H $_2$ could have been pulled out from the SMC via tidal interactions, but some also could have formed *in situ* in dense clouds where formation of molecules occurs faster. These dense clouds are possible sites of star formation.

Finally, this study has confirmed the results of Lehner, Keenan, & Sembach (2001) that the HVC at $\sim 80 \text{ km s}^{-1}$ is mainly ionized, but high ions are also associated with it. The high ion ratios are consistent with a radiatively cooling gas in a fountain flow model. Such a model provides an explanation for the origin of HVCs in the low Galactic halo with positive velocity. Alternative scenarios would require a combination of conductive interfaces and turbulent mixing layers.

I thank the FUSE PI team for making these observations possible. I am grateful to Alex Fullerton for a careful reading of the manuscript and for reprocessing the *FUSE* data. I thank Chris Howk for insightful suggestions and discus-

sions. The HST/STIS and AAT observations were obtained by Francis P. Keenan and collaborators at Queen's University of Belfast. This work is based on data obtained for the Guaranteed Time Team by the NASA-CNES-CSA FUSE mission operated by the Johns Hopkins University. Financial support to U. S. participants has been provided by NASA contract NAS5-32985. This work is partly based on observations made with the NASA/ESA Hubble Space Telescope, obtained from the Data Archive at the Space Telescope Science Institute, which is operated by the Association of Universities for Research in Astronomy, Inc., under NASA contract NAS 5-26555. This research has made use of the NASA Astrophysics Data System Abstract Service.

APPENDIX

Spitzer, Cochran, & Hirshfeld (1974) found that for relatively low H_2 column density in the Galaxy, $N(J=0) \lesssim 10^{15} \text{ cm}^{-2}$, a single straight line with a slope characterized by T_{ex} generally fits all the observed levels $J=0, \dots, 3$ or $J=0, \dots, 4$. At slightly higher column densities, $10^{15} \lesssim N(J=0) \lesssim 10^{15.5} \text{ cm}^{-2}$, two excitation temperatures are needed. This was also confirmed by Jenkins et al. (2000b) toward $\epsilon \text{ Ori}$. In their survey, Spitzer, Cochran, & Hirshfeld (1974) have 10 stars with $N(J=0) < 10^{15} \text{ cm}^{-2}$ and two with $10^{15} < N(J=0) \lesssim 10^{15.5} \text{ cm}^{-2}$. At higher column densities, two temperatures are generally needed to describe the populations in the different J levels. This is understood as a consequence of the density being high enough to ensure that collisions dominate over radiative processes for low J ($\lesssim 1$) levels, which couples the levels with the kinetic temperature. For higher J ($\gtrsim 4$), fluorescent pumping dominates and yields a higher excitation temperature, whereas intermediate rotational levels ($J=2, 3$) are fixed by the rate of ultraviolet-pumping or can also be deexcited by collisions due to their longer radiative lifetimes (Shull & Beckwith 1982).

Recently, Tumlinson et al. (2002) used *FUSE* to measure the H_2 column densities for different levels J in the SMC and LMC. For comparison with the Magellanic Bridge and the Galaxy, we reproduced here their measurements for $N(J=0) \lesssim 10^{15.5}$. We summarize the results in the form of an excitation diagram in Figure 12 for 9 and 11 sight lines in the LMC and SMC, respectively. In this Figure, the observed $N(J)$ are plotted with their 1σ error bars estimated by Tumlinson et al. (2002). We indicate the excitation temperature of the first two levels, T_{01} , derived directly from Equation 1, and we plot the resulting *dotted* line with a slope characterized by T_{01} . The data were then fitted using a least-squares method by minimizing the χ^2 error. The number of levels $j+1$ fitted simultaneously is indicated in Figure 12 by T_{0j} ($j > 1$). When the goodness of fit was reasonable, the *dashed* line in Figure 12 shows the result from this least-squares fit; when no *dashed* line is indicated, a proper straight line could not be fitted within the estimated error bars. For reference we have also indicated in this Figure the molecular fraction f_{H_2} , where both the H I and total H_2 column density are given in Tumlinson et al. (2002). The H I column density is derived from the 21 cm emission line and can be quite uncertain. These authors estimated that the error on H I was at least 33%. When the upper-error on H_2 column density is large, f_{H_2} should be considered a lower limit. Within the errors, f_{H_2} is similar to the Galactic value (Savage et al. 1977) for similar total H_2 column density.

Two main conclusions can be directly drawn from Figure 12. (i) Not all the sight lines can be fitted with a single straight-line (Sk $-65^\circ 22$, AV 83, NGC346-3, Sk 188) and some are just at the edge of the error (NGC346-4, AV 327). (ii) When levels $J=0, j$ ($j > 2$) can be fitted with a straight-line, it is not generally the case that *all* the observed levels can be fitted with the same line (SK $-67^\circ 69$, BI 173, Sk $-67^\circ 166$, HD 269927, NGC346-6, Sk 82, AV 378), i.e., at least two excitation temperatures are sometimes needed to describe properly the distribution of the data points even when $N(J=0) < 10^{15} \text{ cm}^{-2}$. A single excitation temperature could reproduce the observed distribution if either the $J=0$ level was less populated or the $J=1$ level more populated, which would imply in both cases similar excitation temperatures to those observed in the Galaxy. This suggests non-equilibrium of the ortho to para ratio. Note that toward BI 173 and HD 269927 the $J=4$ level would still seem to be overpopulated to allow a single excitation temperature to fit the observed distribution.

The future H_2 Galactic survey with *FUSE* coupled with refined models and the Magellanic Clouds survey should improve our understanding of H_2 in low density diffuse gas with different metallicities.

REFERENCES

- Abgrall, H., Roueff, E., Launay, F., Roncin, J. Y., & Subtil, J. L. 1993a, A&AS, 101, 273
 Abgrall, H., Roueff, E., Launay, F., Roncin, J. Y., & Subtil, J. L. 1993b, A&AS, 101, 323
 Anders, E., & Grevesse, N., 1989, Geochim. Cosmochim. Acta, 53, 197
 Barnes, J. E., & Hernquist, L. 1992, ARA&A, 30, 705
 Borkowski, K. J., Balbus, S. A., & Frstrom, C. C. 1990, ApJ, 355, 501
 Christodoulou, D. M., Tohline, J. E., & Keenan, F. P. 1997, ApJ, 468, 810
 Demers, S., & Battinelli, P. 1998 AJ, 115, 154
 Evans, N. J. II 1999, ARA&A, 37, 311
 Fitzpatrick, E. L. 1996, ApJ, 473, L55
 Grevesse, N., & Noels, A. 1993, in Origin of the Elements, ed. N. Prantzos et al. (Cambridge: Cambridge Univ. Press), 15
 Gardiner, L. T., & Noguchi, M. 1996, MNRAS, 278, 191

- Garnett, D. R. 1999, in IAU no. 190 New Views of the Magellanic Clouds, ed. Y.-H. Chu et al., p.266
- Gibson, B. K., Giroux, M. L., Penton, S. V., Putman, M. E., Stocke, J. T., & Shull, J. M. 2000, *AJ*, 120, 1830
- Hambly, N. C., Dufton, P. L., Keenan, F. P., Rolleston, W. R. J., Howarth, I. D., Irwin, M. J. 1994, *A&A*, 285, 716
- Henry, R. B. C., & Worthey, G. 1999 *PASP*, 111, 919
- Henry, R. B. C., Edmunds, M. G., & Köppen, J. 2000 *ApJ*, 163, 165
- Hollenbach, D. J., Werner, M. W., & Salpeter, E. E. 1971 *ApJ*, 163, 165
- Hoopes, C. G., Sembach, K. R., Howk, J. C., Savage, B. D., & Fullerton, A. W. 2002, *ApJ*, 569, 233
- Howk, J. C., Sembach, K. R., Roth, K. C., & Kruk, J. W. 2000, *ApJ*, 544, 867
- Howk, J. C., Savage, B. D., Sembach, K. R., & Hoopes, C. G. 2002b, *ApJ*, in press
- Howk, J. C., Sembach, K. R., Savage, B. D., Massa, D., Friedman, S. D., & Fullerton, A. W. 2002a, *ApJ*, 569, 214
- Irwin, M. J., Demers, S., Kunkel, W. E. 1990, *AJ*, 99, 191
- Jenkins, E. B. 1987, in *Interstellar Processes*, edd. D.J. Hollenbach & H.A. Thronson (Dordrecht: Reidel), 533
- Jenkins, E. B., et al. 2000a, *ApJ*, 538, L81
- Jenkins, E. B., Woźniak, P. R., Sofia, U. J., Sonneborn, G., & Tripp, T. M. 2000b, *ApJ*, 538, 275
- Kobulnicky, H. A., & Dickey, J. M. 1999, *AJ*, 117, 908
- Korn, A. J., & Wolf, B. 1999, in IAU no. 190 New Views of the Magellanic Clouds, ed. Y.-H. Chu et al., p.241
- Lauroesch, J. T., Truran, J. W., Welty, D. E., & York, D. G. 1996, *PASP*, 108, 641
- Lehner, N. 2000, PhD Thesis, The Queen's University of Belfast
- Lehner, N., Fullerton, A. W., Sembach, K. R., Massa, D., Jenkins, E. B. 2001c, *ApJ*, 556, L103
- Lehner, N., Keenan, F.P., & Sembach, K. R. 2001, *MNRAS*, 323, 904
- Lehner, N., Sembach, K. R., Dufton, P. L., Rolleston, W. J. R., & Keenan, F. P. 2001, *ApJ*, 551, 781
- Lehner, N., Sembach, K. R., Lambert, D. L., Ryans, R. S. I., & Keenan, F. P. 1999, *A&A*, 352, 257
- Lu, L., Sargent, W. L. W., & Barlow, T. A. 1998b, *AJ*, 115, 55
- Lu, L., Savage, B. D., Sembach, K. R., Wakker, B. P., Sargent, W. L. W., & Oosterloo, T. A. 1998, *AJ*, 115, 162
- Mallouris, C., et al. 2001 *ApJ*, 558, 133
- Meyer, D. M., Jura, M., & Cardelli, J. A. 1998, *ApJ*, 493, 222
- Moos, H. W., et al. 2000, *ApJ*, 538, L1
- Morton, D. C. 1991, *ApJS*, 77, 119
- Prochaska, J. X., Henry, R. B. C., O'Meara, J. M., Tytler, D., Wolfe, A. M., Kirkman, D., Lubin, D., & Suzuki, N., 2002 *ApJ*, submitted
- Putman, M. E. 2000, *PASA*, 17, 1
- Putman, M. E., Staveley-Smith, L., Freeman, K. C., Gibson, B. K., & Barnes, D. G. 2002, *ApJ*, to be submitted
- Richter, P., Sembach, K.R., Wakker, B.P., & Savage, B.D. 2001, *ApJ*, 526, L181
- Rolleston, W. R. J., Dufton, P. L., McErlean, N. D., & Venn, K. A. 1999, *A&A*, 348, 728
- Russell, S. C., & Dopita, M. A. 1992, *ApJ*, 384, 508
- Sahnow, D. J., et al. 2000, *ApJ*, 538, L7
- Savage, B. D., Bohlin, R. C., Drake J. F., & Budich, W. 1977, *ApJ*, 216, 291
- Savage, B. D., & Sembach, K. R. 1991, *ApJ*, 379, 245
- Savage, B. D., & Sembach, K. R. 1996, *ARA&A*, 34, 279
- Savage, B. D. et al., 2000, *ApJ*, 538, L30
- Scoville, N. Z., Sanders, D. B., & Clemens, D. P. 1986, *ApJ*, 310, L77
- Sembach, K. R., Howk, J. C., Ryans, R. S. I., & Keenan, F. P. 2000, *ApJ*, 528, 310
- Sembach, K. R., Howk, J. C., Savage, B. D., & Shull J. M. 2001, *ApJ*, 121, 992
- Sembach, K. R., & Savage, B. D. 1992, *ApJS*, 83, 147
- Sembach, K. R., & Savage, B. D., Hurwitz, M. 1999, *ApJ*, 524, 98
- Shull, J. M., & Beckwith, S. 1979, *ApJ*, 227, 131
- Shull, J. M., & McKee, C.F. 1979, *ApJ*, 227, 131
- Shull, J. M., et al. 2000, *ApJ*, 538, L73
- Slavin, J. D., Shull, J. M., & Begelman, M. C. 1993, *ApJ*, 407, 83
- Smoker, J.V., Keenan, F.P., Polatidis, A., Mooney, C.J., Lehner, N., & Rolleston, W.R.J. 2000, *A&A*, 363, 451
- Sofia, U. J., & Jenkins, E. B. 1998, *ApJ*, 499, 951
- Spitzer, L. 1996, *ApJ*, 458, L29
- Spitzer, L., Cochran, W. D., & Hirshfeld, A. 1974, *ApJS*, 28, 373
- Sutherland, R. S., & Dopita, M. A. 1993, *ApJS*, 88, 253
- Tripp, T. M., & Savage, B. D. 2000, *ApJ*, 542, 42
- Tumlinson, J., et al. 2002, *ApJ*, 566, 857
- Vila-Costa, M. B., & Edmunds, M. G. 1993, *MNRAS*, 265, 199
- Wakker, B. P., & van Woerden, H., 1997, *ARA&A*, 35, 217
- Welty, D. E., Lauroesch, J. T., Blades, J. C., Hobbs, L. M., & York, D. G. 1997, *ApJ*, 489, 672
- Welty, D. E., Frisch, P. C., Sonneborn, G., & York, D. G. 1999a, *ApJ*, 512, 636
- Welty, D. E., Hobbs, L. M., Lauroesch, J. T., Morton, D. C., Spitzer, L., & York, D. G. 1999b, *ApJS*, 124, 465
- Wiese, L. M., Bonvallet, G. A., & Lawler, J. E. 2002, *ApJ*, 569, 1032
- Zsargó, J., Sembach, K. R., Howk, J. C., & Savage, B. D. 2002, *ApJ*, in preparation

TABLE 1
 ATMOSPHERIC AND OTHER OBSERVATIONAL PARAMETERS OF DI 1388 AND DGIK 975

Star	α (J2000)	δ (J2000)	V	$B - V$	T_{eff} kK	$\log g$ dex	v_t km s^{-1}	v_{LSR}^* km s^{-1}	$v \sin i$ km s^{-1}
DI 1388	02:57:11.94	-72:52:54.61	14.39	-0.26	32	4.0	5	150	180
DGIK 975	04:19:58.63	-73:52:25.80	15.05	-0.12	20	3.6	5	210	80

Note. — Results are from Hambly et al. (1994) (DI 1388) and Rolleston et al. (1999) (DGIK 975) and references therein.

TABLE 2
ATOMIC AND MOLECULAR ABSORPTION LINES IN FUSE SPECTRA TOWARD DI 1388

Species	λ_{lab}^a (Å)	f^a	S/N ^b	W_λ (mÅ)	$\log N$ (cm ⁻²)	Note
C III	977.020	7.62×10^{-1}	24	182.0 ± 15.1	> 13.76	
N I	953.655	2.50×10^{-2}	9	20.2 ± 9.2	$14.07 \pm_{0.26}^{0.17}$	
	953.970	3.48×10^{-2}	10	16.8 :	13.90 :	
	954.104	6.76×10^{-3}	9	< 18	< 14.52	
	964.626	9.43×10^{-3}	9	8.5 :	14.05 :	
	1134.415	2.97×10^{-2}	38	26.5 ± 2.8	> 13.97	
	1134.980	4.35×10^{-2}	18	33.3 ± 4.9	> 13.93	
N II	1083.994	1.15×10^{-1}	12	118.9 ± 9.3	> 14.19	
N III	989.799	1.23×10^{-1}	7	136 ± 22	13.5 :	1
O I	924.950	1.54×10^{-3}	10	< 22	< 15.28	
	929.517	2.29×10^{-3}	13	21.8 ± 3.9	15.31 ± 0.17	2
	936.630	3.65×10^{-3}	19	34.9 ± 4.4	15.18 ± 0.06	
	948.686	6.31×10^{-3}	9	43 ± 20	$> 15.04 :$	
	950.885	1.58×10^{-3}	16	24.4 ± 7.0	15.36 :	3
	1039.230	9.20×10^{-3}	20	60.4 ± 5.4	> 14.96	
P II	1152.818	2.45×10^{-1}	19	5.7 :	12.34 :	
S III	1012.495	4.43×10^{-2}	22	14.3 ± 4.0	$13.58 \pm_{0.15}^{0.11}$	
Ar I	1048.220	2.63×10^{-1}	30	5.6 ± 1.4	$12.39 \pm_{0.13}^{0.09}$	
	1066.660	6.65×10^{-2}	23	< 9	< 13.1	
Fe II	1055.262	7.50×10^{-3}	24	7.9 ± 3.9	$14.05 \pm_{0.27}^{0.17}$	
	1063.176	5.47×10^{-2}	32	40.1 ± 3.8	13.92 ± 0.05	
	1096.877	3.20×10^{-2}	22	25.8 ± 5.5	$13.93 \pm_{0.12}^{0.09}$	
	1125.448	1.60×10^{-2}	32	15.8 ± 7.8	$13.97 \pm_{0.30}^{0.17}$	
	1143.226	1.77×10^{-2}	32	14.1 ± 3.3	13.87 ± 0.10	
	1144.938	1.06×10^{-1}	24	73.0 ± 4.6	13.90 ± 0.03	
Fe III	1122.524	5.44×10^{-2}	24	24.5 ± 3.7	13.66 ± 0.07	
H ₂ $J = 0$						
1-0 $R(0)$	1092.195	5.90×10^{-3}	17	20.6 ± 5.2	14.88 ± 0.30	
3-0 $R(0)$	1062.882	1.79×10^{-2}	16	32.3 ± 6.9	...	
H ₂ $J = 1$						
0-0 $Q(1)^a$	1009.771	2.38×10^{-2}	15	31.5 ± 3.6	15.05 ± 0.07	
0-0 $R(1)$	1108.633	1.08×10^{-3}	15	10.1 ± 4.4	...	
1-0 $R(1)$	1092.732	3.78×10^{-3}	19	19.6 ± 4.4	...	
2-0 $R(1)$	1077.697	7.84×10^{-3}	16	25.5 ± 4.4	...	
3-0 $R(1)$	1063.460	1.19×10^{-2}	16	25.8 ± 2.2	...	
4-0 $R(1)$	1049.960	1.56×10^{-2}	16	32.4 ± 4.8	...	
7-0 $R(1)$	1013.435	2.05×10^{-2}	16	28.4 ± 4.1	...	
8-0 $R(1)$	1002.449	1.82×10^{-2}	22	32.0 ± 4.3	...	
1-0 $P(1)$	1094.052	1.97×10^{-3}	19	14.3 ± 4.9	...	
2-0 $P(1)$	1078.923	3.90×10^{-3}	17	26.9 ± 7.2	...	
3-0 $P(1)$	1064.606	5.66×10^{-3}	12	22.3 ± 7.3	...	
4-0 $P(1)$	1051.031	7.73×10^{-3}	26	27.1 ± 3.8	...	
H ₂ $J = 2$						
0-0 $Q(2)$	1010.938	2.45×10^{-2}	18	21.0 ± 3.5	$14.60 \pm_{0.16}^{0.22}$	
1-0 $R(2)$	1094.244	3.31×10^{-3}	15	6.5 ± 4.6	...	
4-0 $R(2)$	1051.498	1.40×10^{-2}	23	23.0 ± 3.5	...	
8-0 $R(2)$	1003.984	1.67×10^{-2}	13	21.3 ± 4.4	...	
10-0 $R(2)$	983.589	1.16×10^{-2}	12	19.8 ± 5.2	...	
1-0 $R(2)^a$	986.241	2.62×10^{-2}	11	26.5 ± 5.2	...	
H ₂ $J = 3$						
0-0 $P(3)$	1014.504	8.28×10^{-3}	16	17.8 ± 4.6	$14.58 \pm_{0.08}^{0.13}$	

TABLE 2—*Continued*

Species	λ_{lab}^a (Å)	f^a	S/N ^b	W_λ (mÅ)	$\log N$ (cm ⁻²)	Note
4-0 <i>P</i> (3)	1056.472	9.56×10^{-3}	25	18.0 ± 3.0	...	
1-0 <i>R</i> (3) ^a	987.445	2.57×10^{-2}	12	24.7 ± 4.6	...	
H ₂ <i>J</i> = 4						
3-0 <i>R</i> (4)	1070.899	9.67×10^{-3}	20	< 11	< 14.0	

Note. — Uncertainties are 1σ errors. Upper limits indicate that no feature is present and are 3σ estimates. Lower limits indicate that the absorption line is saturated. Colons indicate that the value is uncertain. For atomic species, the column density is the direct integration of the apparent column density; while for H₂, it results from a COG analysis. Note however that the adopted column densities for N I, O I, and Fe II result from a COG analysis, see Table 7 and § 3.

(a) Rest frame vacuum wavelengths and oscillator strengths are from Morton (private communication, 2000) for the atomic and ionic species, except for the f -values of Fe II which are from Howk et al. (2000). The H₂ wavelengths are from Abgrall et al. (1993a,b), while the H₂ f -values were calculated from the emission probabilities given by those authors. (b) Signal-to-noise level per spectral resolution.

(1) N III λ 989.8 is blended with Si II λ 989.9. The equivalent width is the total strength of this feature (N III and Si II). To obtain the column density, the contribution of Si II to the feature was removed (see § 3 for more details). (2) The red wing of the line is blended with local O I. (3) The line is blended with local H₂. (4) Blended with lower velocity components, profile integrated from 160 to 255 km s⁻¹.

TABLE 3

INTERSTELLAR ATOMIC/IONIC ABSORPTION LINES IN *FUSE* SPECTRA TOWARD DGIK 975

Ions	λ_{lab}^a (Å)	f^a	S/N ^b	W_λ (mÅ)	$\log N_a$ (cm ⁻²)
N I	1134.165	1.52×10^{-2}	7	< 30	< 14.2
	1134.980	4.35×10^{-2}	9	31.9 ± 9.7	$13.87 \pm \begin{smallmatrix} 0.17 \\ 0.17 \end{smallmatrix}$
N II	1083.994	1.15×10^{-1}	2
O I	1039.230	9.20×10^{-3}	12	66.4 ± 9.1	> 15.04
Si II	1020.699	1.64×10^{-2}	6	34 :	14.4 :
P II	1152.818	2.45×10^{-1}	8	< 26	< 13.0
Ar I	1048.220	2.63×10^{-1}	10	< 21	< 12.9
Fe II	1096.877	3.20×10^{-2}	9	47.9 ± 13.7	$14.21 \pm \begin{smallmatrix} 0.11 \\ 0.15 \end{smallmatrix}$
	1125.448	1.60×10^{-2}	12	23.6 ± 6.2	$14.20 \pm \begin{smallmatrix} 0.10 \\ 0.13 \end{smallmatrix}$
	1143.226	1.77×10^{-2}	7	43.3 :	14.39 :
	1144.938	1.06×10^{-1}	7	140 ± 18	14.22 ± 0.10
Fe III	1122.524	5.44×10^{-2}	7	90.4 ± 39.0	$14.27 \pm \begin{smallmatrix} 0.16 \\ 0.25 \end{smallmatrix}$

Note. — Uncertainties are 1σ errors. Upper limits indicate that no feature is present and are 3σ estimates. Lower limits indicate that the absorption line is saturated. Colons indicate that the value is uncertain.

(a) Rest frame vacuum wavelengths and oscillator strengths are from Morton (private communication, 2000), except for the f -values of Fe II which are from Howk et al. (2000). (b) Signal-to-noise level per spectral resolution.

TABLE 4
HIGHLY IONIZED SPECIES TOWARD DI 1388

Species	λ_{lab}^a (Å)	f^a	$\log N$ (cm^{-2}) MB [155, 245] ^c	$\log N$ (cm^{-2}) MB [100, 245] ^c	$\log N$ (cm^{-2}) HVC [70, 100] ^c	$\log N$ (cm^{-2}) MW [-40, 40] ^c	Fit ^b
O VI	1031.926	1.32×10^{-1}	13.13 ± 0.16	13.59 ± 0.10	13.18 ± 0.12	14.08 ± 0.05	P
C IV	1548.195	1.90×10^{-1}	13.27 ± 0.06	13.36 ± 0.10	P
	1550.770	9.52×10^{-2}	13.25 ± 0.07	13.28 ± 0.10	$12.33 \pm \begin{smallmatrix} 0.15 \\ 0.23 \end{smallmatrix}$	13.88 ± 0.03	G
			13.34 ± 0.13	13.40 ± 0.15	$12.45 \pm \begin{smallmatrix} 0.23 \\ 0.50 \end{smallmatrix}$	13.89 ± 0.03	P
			13.33 :	13.54 :	12.98 :	13.97 ± 0.10	P
Si IV	1393.755	5.14×10^{-1}	12.87 ± 0.06	...	11.91 ± 0.13	13.21 ± 0.04	G
			12.92 ± 0.06	13.02 ± 0.08	12.18 ± 0.15	13.20 ± 0.04	P
			12.99 ± 0.06	13.18 ± 0.08	12.48 ± 0.10	13.27 ± 0.04	P
	1402.770	2.55×10^{-1}	12.92 ± 0.06	13.29 ± 0.04	G
			12.90 ± 0.05	12.97 ± 0.15	12.20 ± 0.20	13.29 ± 0.04	P
			13.17 ± 0.06	13.40 ± 0.07	12.75 ± 0.11	13.34 ± 0.06	P

Note. — Uncertainties are 1σ errors. Colons indicate that the value is uncertain. (a) Rest frame vacuum wavelengths and oscillator strengths are from Morton (private communication, 2000). (b) Gaussian (G) or polynomial (P) fit to the continuum (see § 4.3 and Figure 7 for more details). (c) Range in km s^{-1} over which the column density profile is integrated.

TABLE 5
ADOPTED COLUMN DENSITIES AND RATIOS OF THE HIGHLY IONIZED SPECIES TOWARD DI 1388

	MB [155, 245]	MB [100, 245]	HVC [70, 100]	MW [-40, 40]
$N(\text{O VI})$	13.13 ± 0.16	13.59 ± 0.10	13.18 ± 0.12	14.08 ± 0.05
$N(\text{C IV})$	$13.29 \pm \begin{smallmatrix} 0.16 \\ 0.07 \end{smallmatrix}$	$13.35 \pm \begin{smallmatrix} 0.20 \\ 0.10 \end{smallmatrix}$	$12.39 \pm \begin{smallmatrix} 0.25 \\ 0.50 \end{smallmatrix}$	13.89 ± 0.03
$N(\text{Si IV})$	$12.93 \pm \begin{smallmatrix} 0.20 \\ 0.07 \end{smallmatrix}$	$13.18 \pm \begin{smallmatrix} 0.20 \\ 0.10 \end{smallmatrix}$	$12.40 \pm \begin{smallmatrix} 0.35 \\ 0.30 \end{smallmatrix}$	13.27 ± 0.07
$N(\text{C IV})/N(\text{O VI})$	$1.5 \pm \begin{smallmatrix} 1.5 \\ 0.6 \end{smallmatrix}$	$0.6 \pm \begin{smallmatrix} 0.5 \\ 0.2 \end{smallmatrix}$	$0.2 \pm \begin{smallmatrix} 0.2 \\ 0.2 \end{smallmatrix}$	$0.6 \pm \begin{smallmatrix} 0.2 \\ 0.1 \end{smallmatrix}$
$N(\text{C IV})/N(\text{Si IV})$	$2.3 \pm \begin{smallmatrix} 1.6 \\ 1.1 \end{smallmatrix}$	$1.5 \pm \begin{smallmatrix} 1.5 \\ 0.8 \end{smallmatrix}$	$1.0 \pm \begin{smallmatrix} 2.5 \\ 0.9 \end{smallmatrix}$	$4.2 \pm \begin{smallmatrix} 1.2 \\ 0.8 \end{smallmatrix}$

Note. — Error bars reflect the range of possible values. Numbers between brackets indicate the range in km s^{-1} over which the column density profile is integrated.

TABLE 6
HIGHLY IONIZED SPECIES TOWARD DGIK 975

	MB	MW
$N(\text{O VI}) (\lambda 1031.926)$	14.26 ± 0.12	$13.70 \pm \begin{smallmatrix} 0.17 \\ 0.27 \end{smallmatrix}$
$N(\text{C IV}) (\lambda 1550.770)$	13.69 ± 0.14	13.90 ± 0.10
$N(\text{Si IV}) (\lambda 1393.755)$	13.42 ± 0.06	13.21 ± 0.07
$N(\text{Si IV}) (\lambda 1402.770)$	13.40 ± 0.13	13.19 ± 0.13
$N(\text{Si IV})$ (mean)	13.41 ± 0.10	13.20 ± 0.10
$N(\text{C IV})/N(\text{O VI})$	0.3 ± 0.1	1.6 ± 0.8
$N(\text{C IV})/N(\text{Si IV})$	1.9 ± 0.8	5.0 ± 1.7

Note. — Uncertainties are 1σ errors.

TABLE 7
SUMMARY OF DEPLETIONS OF THE MB TOWARD DI 1388

Ions	MB			Galactic Depletions			SMC	LMC	Data
	X^i	$\log(\frac{X}{S})_c^a$	$\log(N(X^i))^b$	$D(X)$	Cold ^c	Warm ^c	Halo ^d	$[X/S]^e$	$[X/S]^e$
C II	+1.28	> 14.87	> -0.65	-0.4	-0.4	(-0.4)	-0.14	+0.06	STIS
N I	+0.70	14.20 ± 0.11	$-0.74 \pm \begin{smallmatrix} 0.17 \\ 0.19 \end{smallmatrix}$	-0.1	-0.1	(-0.1)	-0.66	-0.26	<i>FUSE</i> + STIS
O I	+1.60	15.15 ± 0.06	$-0.69 \pm \begin{smallmatrix} 0.14 \\ 0.15 \end{smallmatrix}$	-0.4	-0.4	(-0.4)	-0.16	+0.05	<i>FUSE</i> + STIS
Mg II	+0.31	< 15.00	< +0.45	-1.2	-0.6	-0.3	+0.08	+0.44	STIS
Al II	-0.79	> 12.82	> -0.63	-2.4	-1.1	(-0.6)	+0.20	+0.19	STIS
Si II	+0.28	14.19 ± 0.10	$-0.33 \pm \begin{smallmatrix} 0.16 \\ 0.19 \end{smallmatrix}$	-1.3	-0.4	-0.3	+0.16	+0.02	STIS
P II	-1.70	12.34 :	-0.20 :	-0.5	-0.2	(-0.1)	<i>FUSE</i>
Mn II	-1.74	< 12.78	< +0.28	-1.5	-1.0	-0.7	+0.18	+0.25	STIS
Ar I	-0.71	$12.39 \pm \begin{smallmatrix} 0.09 \\ 0.13 \end{smallmatrix}$	$-1.14 \pm \begin{smallmatrix} 0.19 \\ 0.32 \end{smallmatrix}$	(0.0)	(0.0)	(0.0)	<i>FUSE</i>
Fe II	+0.24	13.94 ± 0.02	-0.54 ± 0.14	-2.2	-1.4	-0.6	+0.01	+0.29	<i>FUSE</i> + STIS
Ni II	-1.02	12.52 ± 0.20	$-0.70 \pm \begin{smallmatrix} 0.22 \\ 0.25 \end{smallmatrix}$	-2.2	-1.4	-0.6	+0.28	+0.36	STIS

Note. — (a) Solar system meteoritic abundances from Anders & Grevesse (1989) except for C, N and O, which are photospheric values from Grevesse & Noels (1993); $\log(S/H)_c = -4.73$. (b) Adopted S II column density, $\log(N(S^+)) = 14.24 \pm 0.13$ dex. The errors on Si II and S II were overestimated by $1/\sqrt{2}$ in Lehner et al. (2001). (c) Updated from Jenkins (1987), see Lauroesch et al. (1996); Welty et al. (1997, 1999b). (d) From Savage & Sembach (1996); Fitzpatrick (1996); and references therein. Values in parentheses are estimated, see Welty et al. (1997, 1999b). For Ni II, the depletions were corrected to take into account the new oscillator strength scaling, see Lehner et al. (2001). (e) $[X/S] = \log(X/S)_{\text{SMC/LMC}} - \log(X/S)_c$ (Russell and Dopita (1992) but adjusted for C, N and O photospheric values, and Al abundances are from Welty et al. (1997, 1999a), while LMC Si abundance is from Korn and Wolf (1999), but see also discussion in Garnett (1999)).

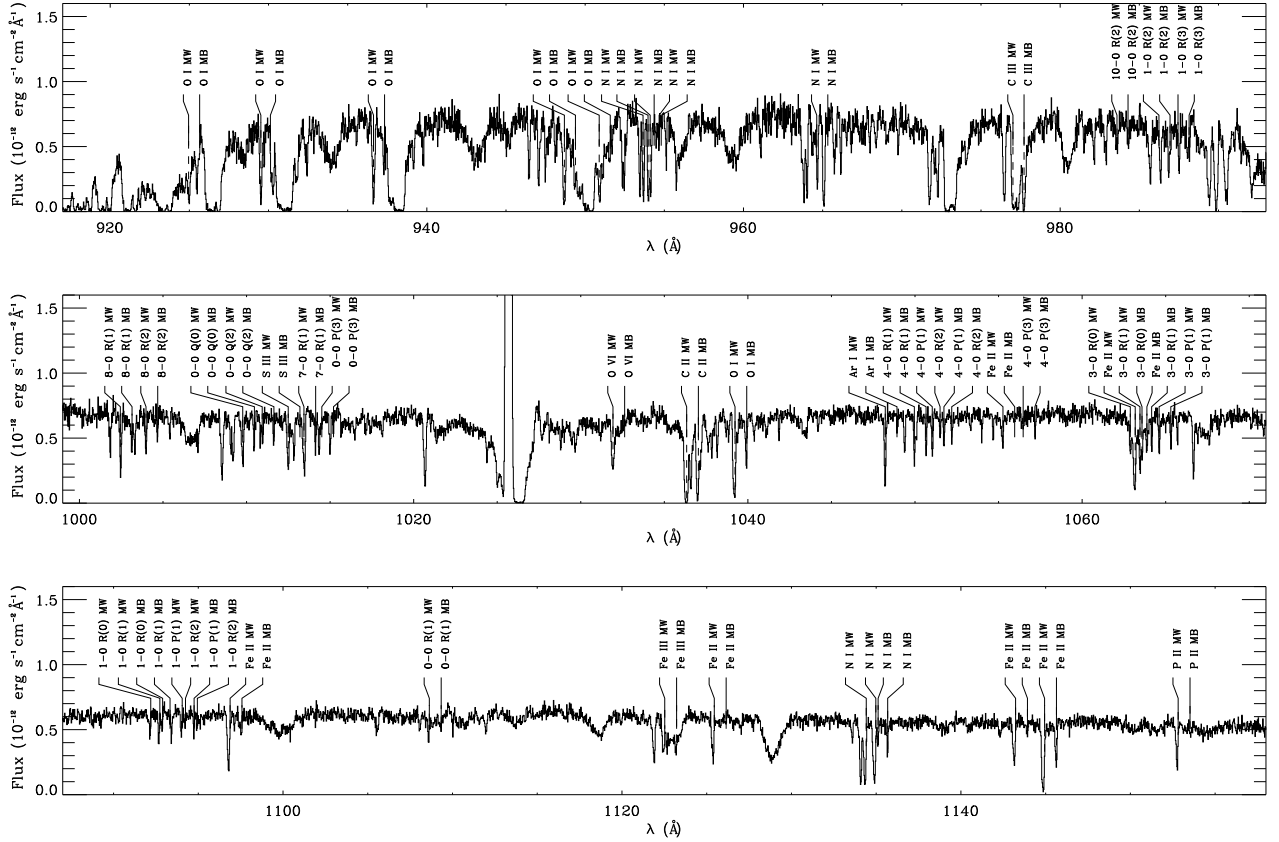


FIG. 1.— Far-ultraviolet spectra of DI 1388 with identification of some interstellar atomic and molecular lines, arising in the Galaxy (MW) and the Magellanic Bridge (MB).

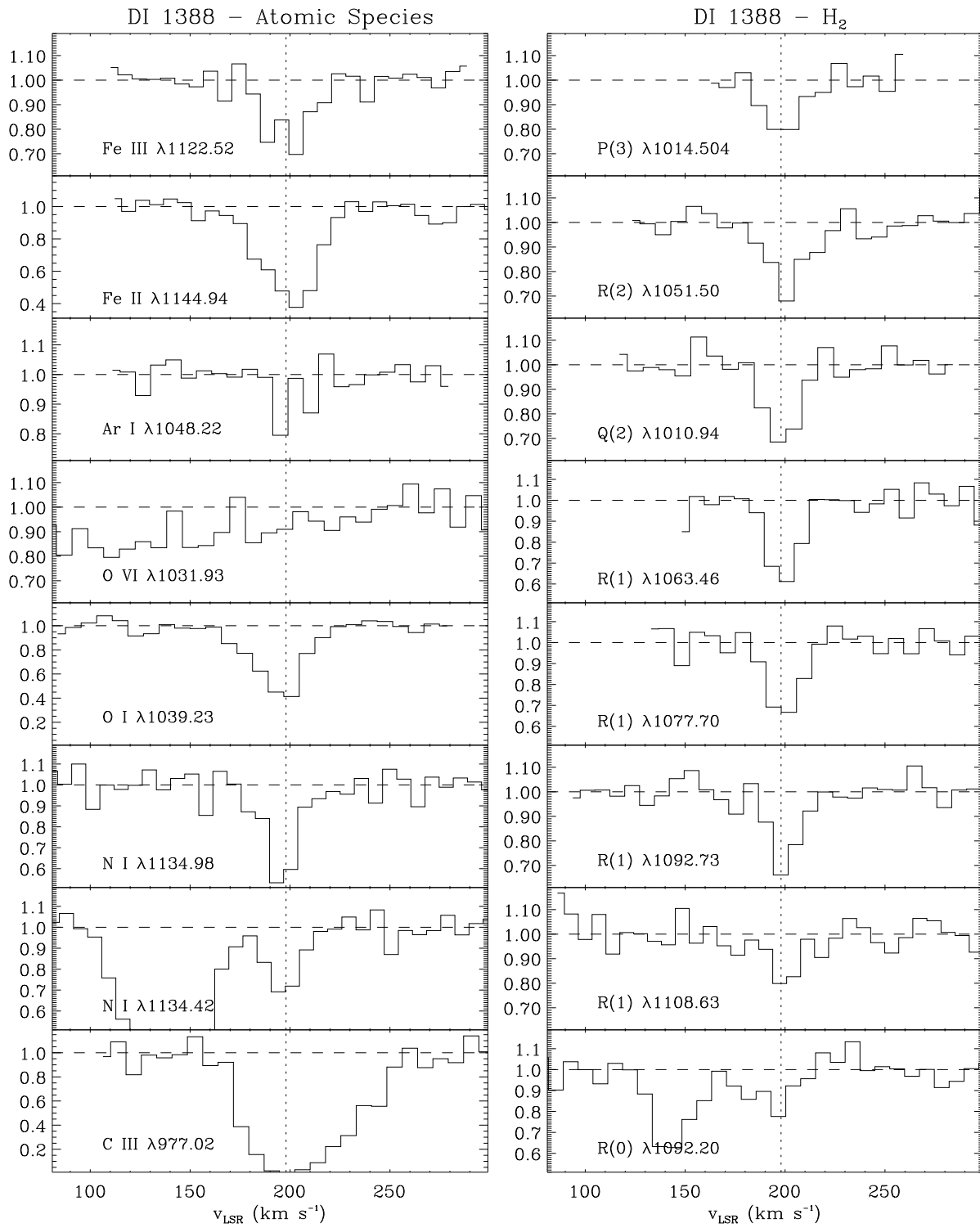


FIG. 2.— Normalized profiles for selected Magellanic Bridge interstellar lines ($v_{\text{LSR}} \sim 200 \text{ km s}^{-1}$) in the DI 1388 spectrum.

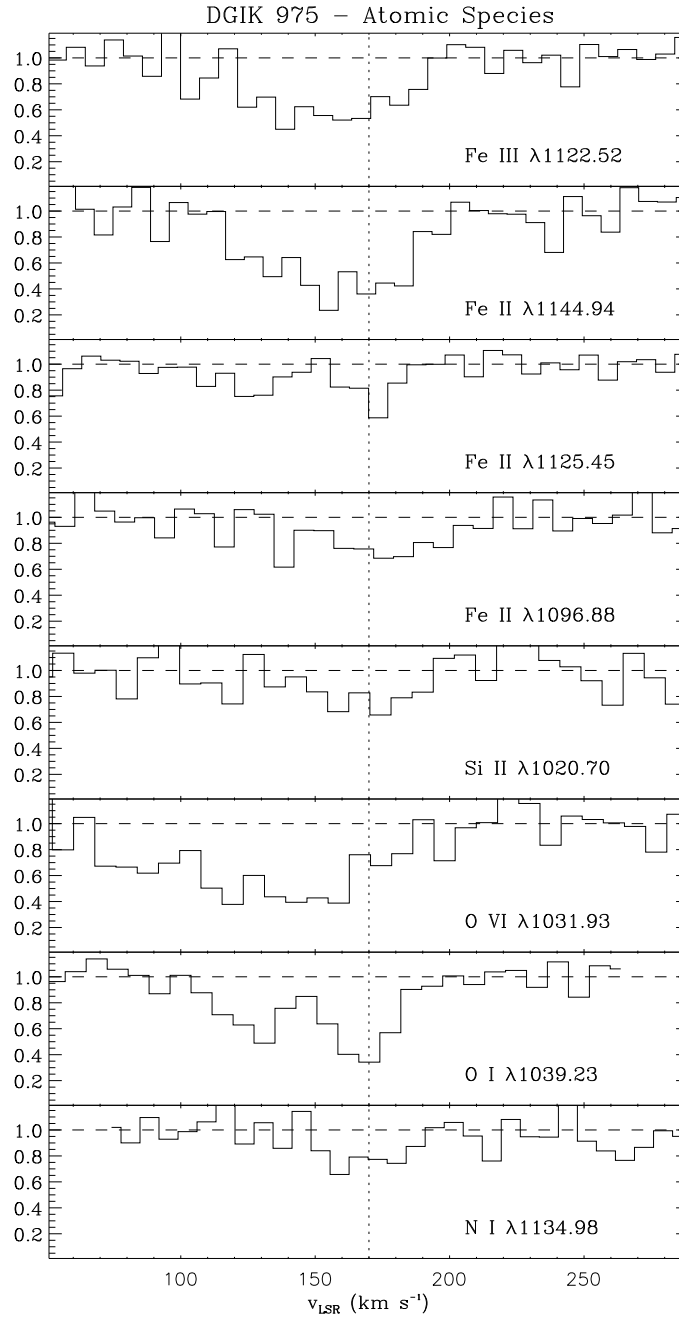


FIG. 3.— Normalized profiles for selected Magellanic Bridge interstellar lines ($v_{\text{LSR}} \sim 170 \text{ km s}^{-1}$) in the DGIK 975 spectrum.

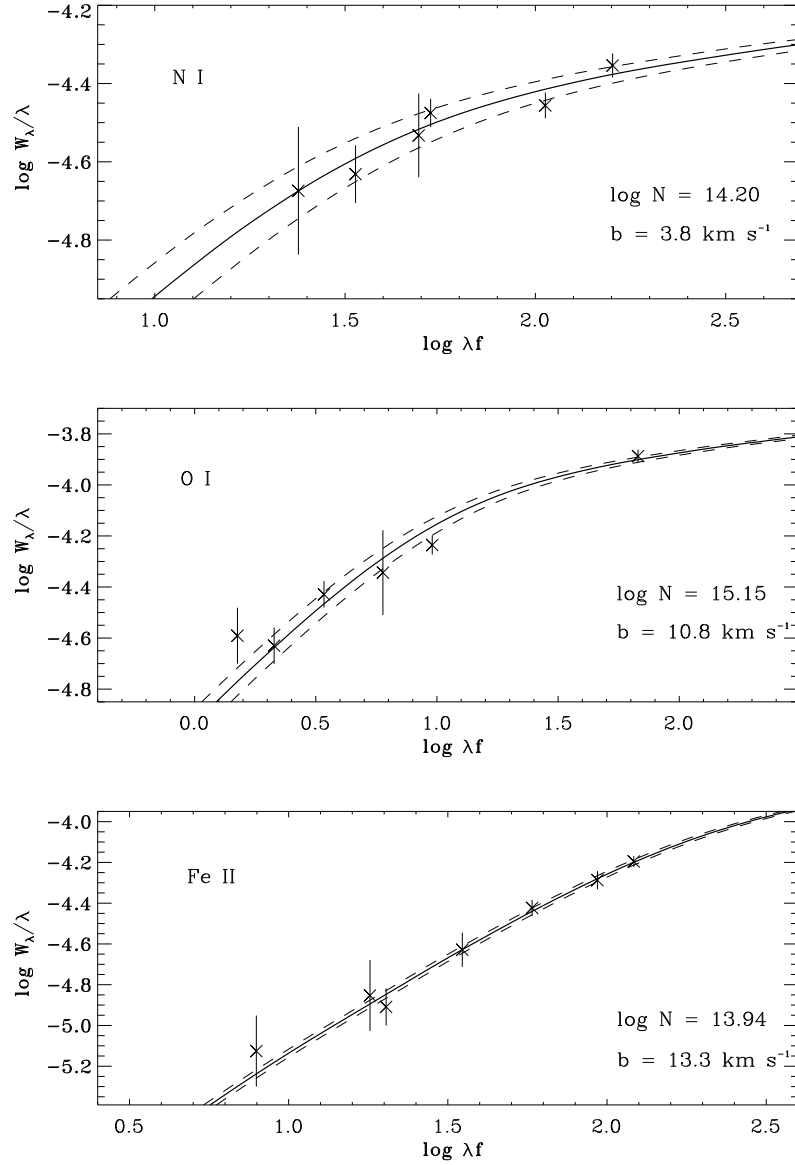


FIG. 4.— Single-component curve of growth for the N I, O I, and Fe II lines identified in the spectrum of DI1388. The dashed lines reflect the 1σ error on the column density.

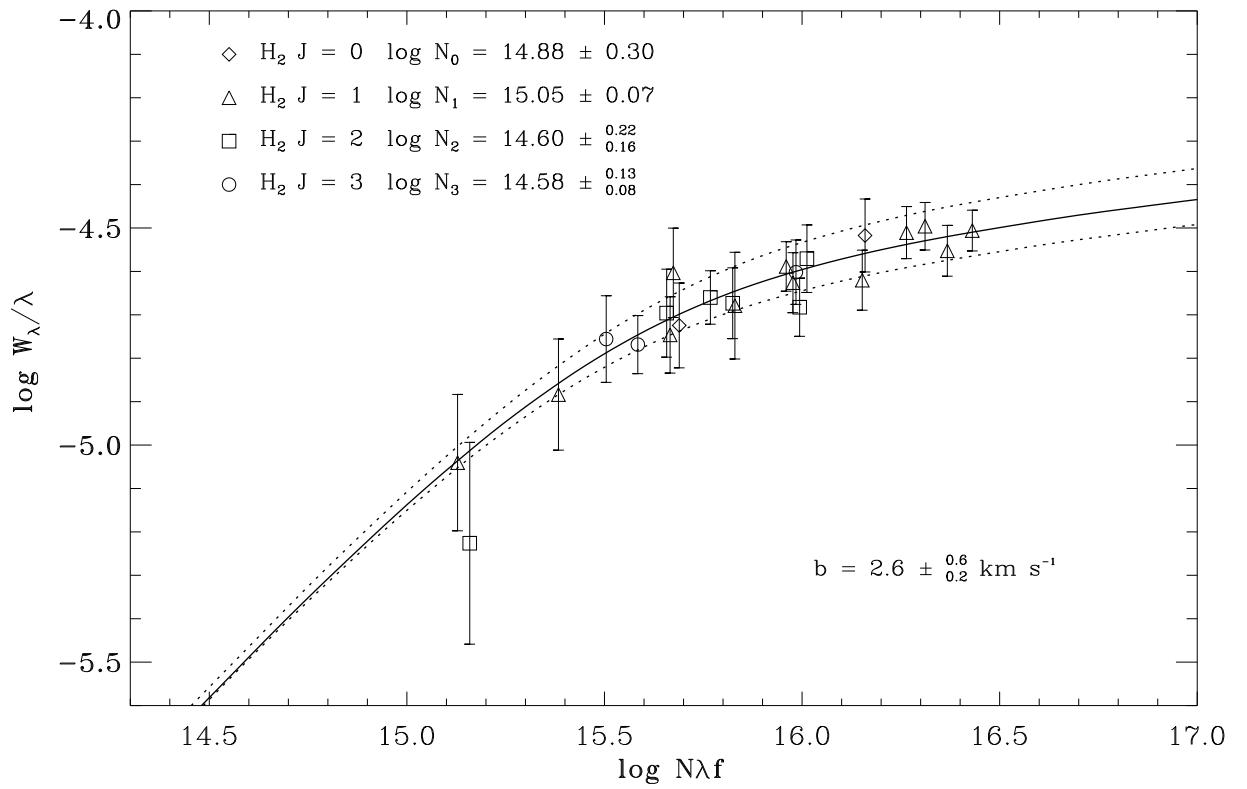


FIG. 5.— Single-component curve of growth for the H₂ lines identified in the spectrum of DI 1388. The dotted lines are the curve of growth for b -values of 2.4 and 3.2 km s⁻¹.

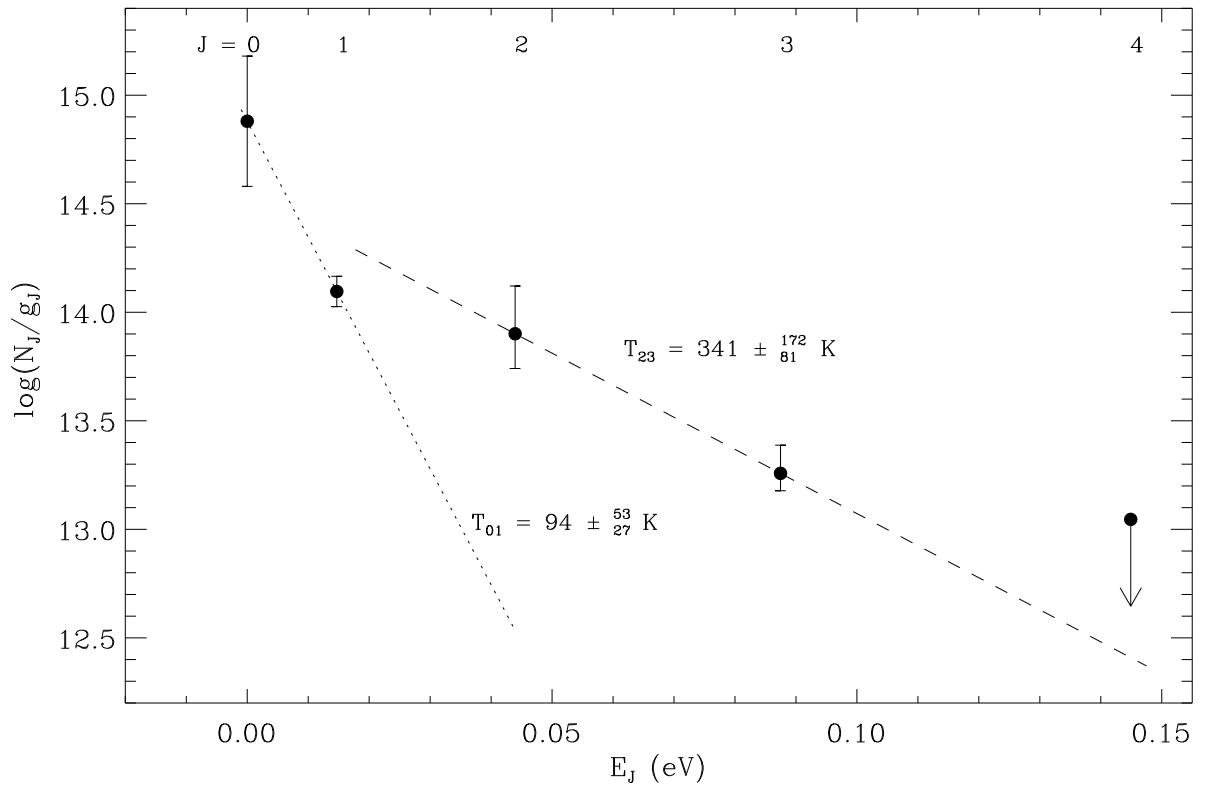


FIG. 6.— H_2 column density (N_J) divided by statistical weight (g_J) as a function of the excitation energy (E_J) for rotational levels $J = 0$ – 4 in the MB toward DI1388. The data point for $J = 4$ is a 3σ upper limit. All other errors are 1σ estimates.

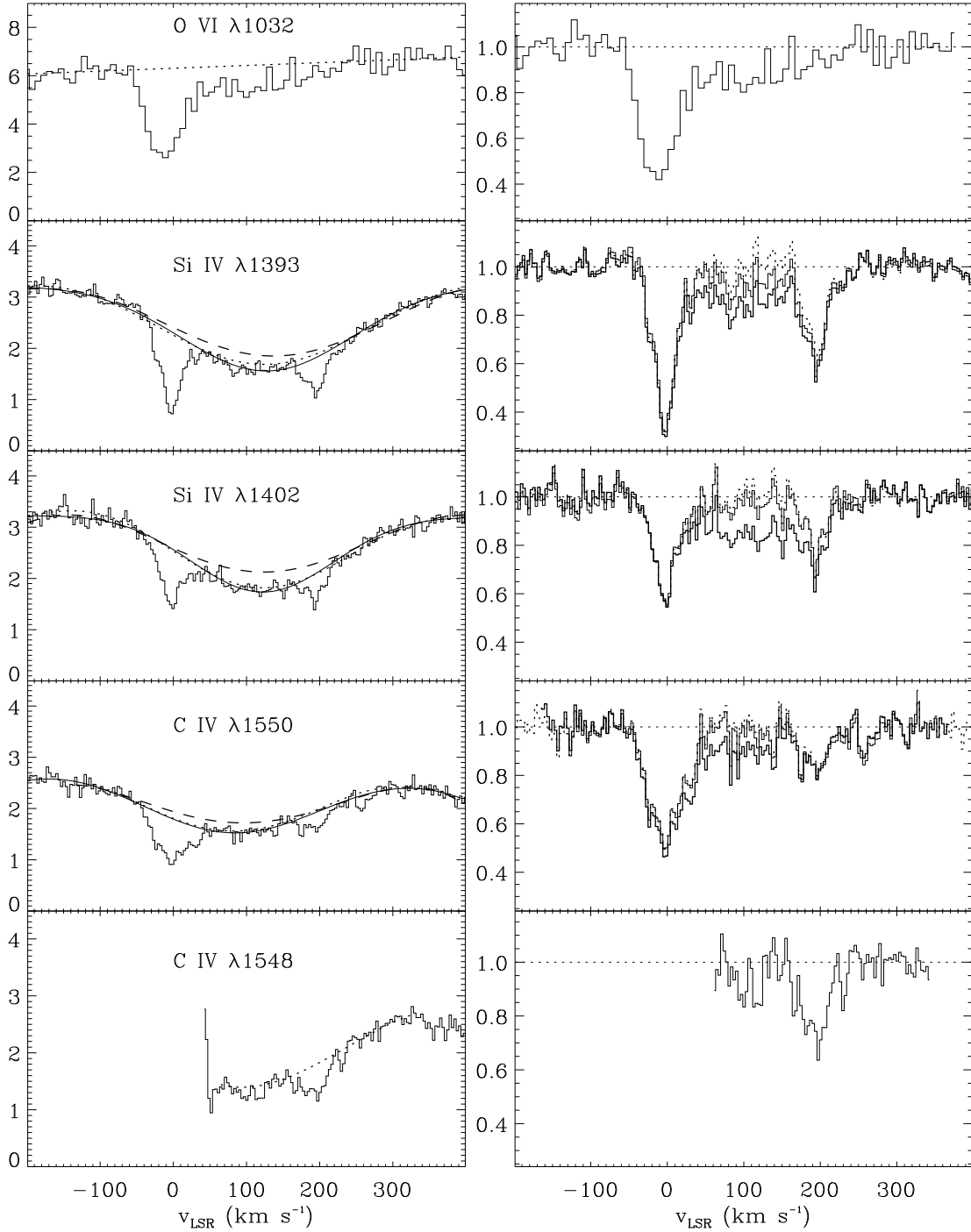


FIG. 7.— Comparison of the highly ionized interstellar species toward DI1388. *Left panel:* Profiles in flux unit ($10^{-13} \text{ erg cm}^{-2} \text{ s}^{-1} \text{ \AA}^{-1}$) versus the LSR velocity. The continua are indicated by the solid line (Gaussian fit), dotted and dashed line (polynomial fit). *Right panel:* Normalized flux versus the LSR velocity. The dotted lines result from the Gaussian fit continuum, while the solid lines result from the polynomial fit continuum.

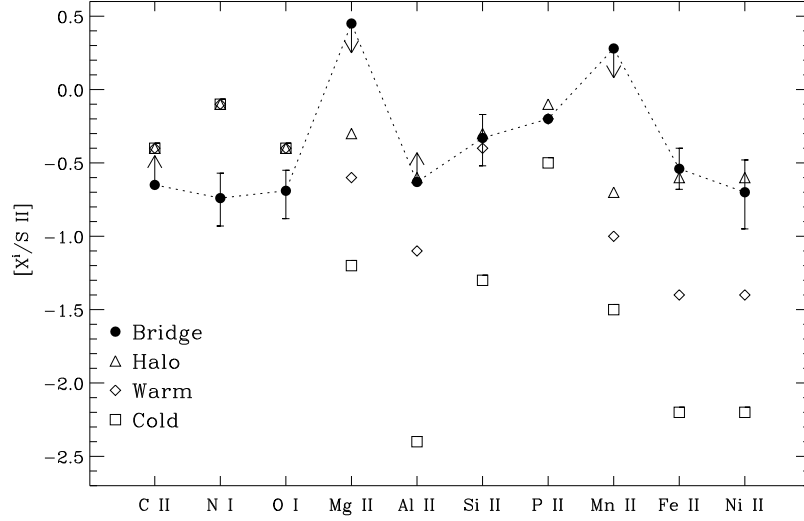


FIG. 8.— Relative gas-phase abundances for the MB (DI1388 sight line), with respect to sulfur (see Table 7), compared to relative abundances found in Galactic cold, warm and halo clouds. Error bars are 1σ . The upward (downward) arrows indicate lower (upper) limits. The value for P II remains uncertain. The dotted line represents the MB depletions corrected from the underlying (undepleted) total elemental relative abundance patterns of the SMC with respect to the Galaxy.

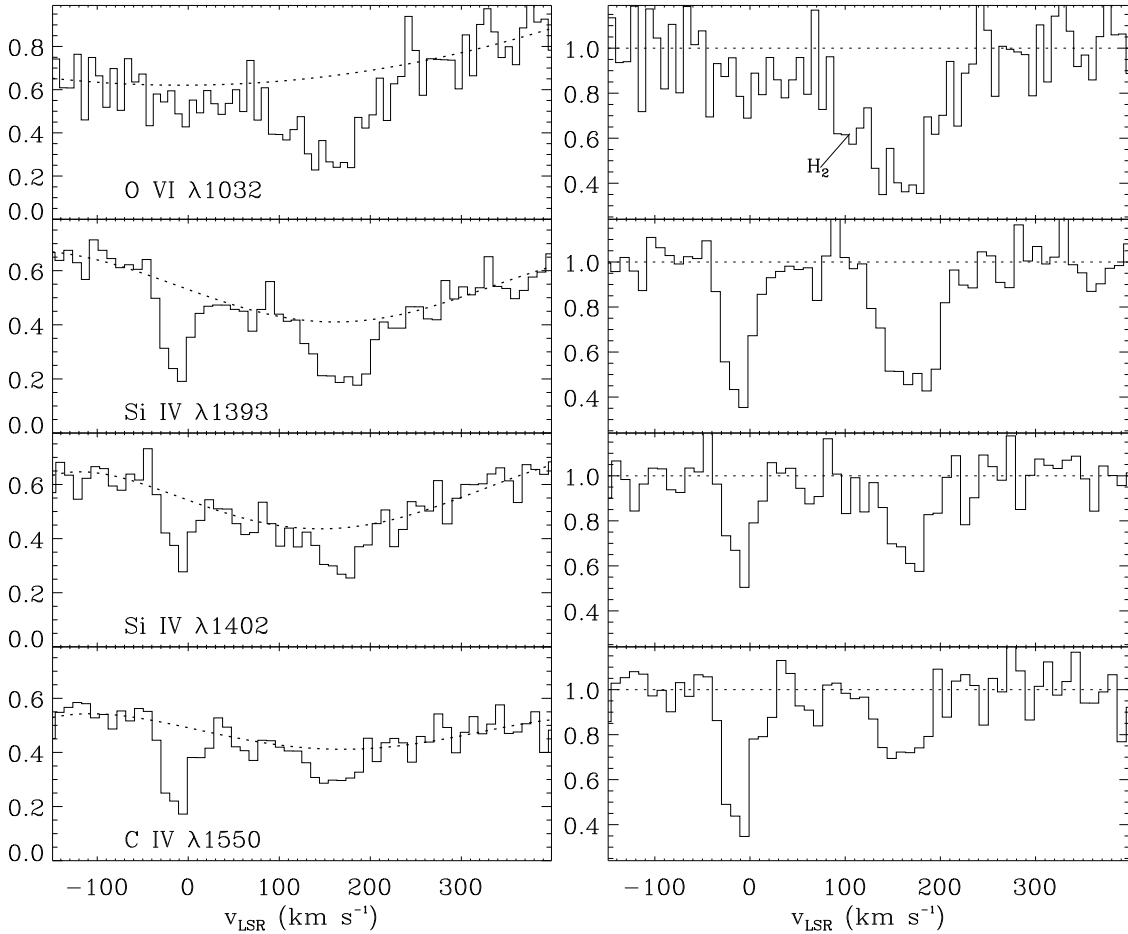


FIG. 9.— Comparison of the highly ionized interstellar species toward DG1K 975. *Left panel:* Profiles in flux unit ($10^{-13} \text{ erg cm}^{-2} \text{ s}^{-1} \text{ \AA}^{-1}$) versus the LSR velocity. The continua are indicated by the dotted line (polynomial fit). *Right panel:* Resulting normalized flux versus the LSR velocity. A possible detection of an highly ionized cloud is observed at $\sim +70 \text{ km s}^{-1}$.

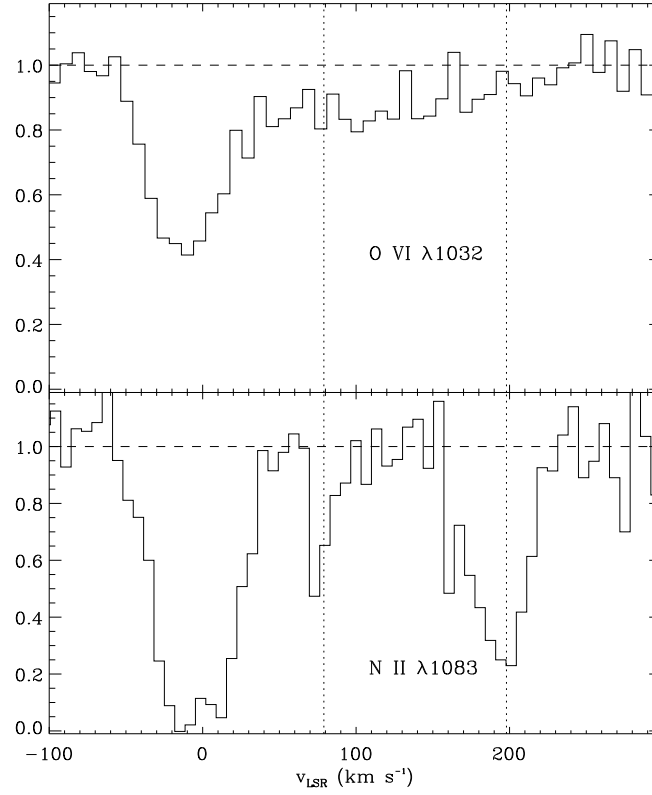


FIG. 10.— Normalized profiles of absorption lines of O VI and N II in the *FUSE* spectrum of DI 1388. Absorption from the Magellanic Bridge is detected at $\sim 200 \text{ km s}^{-1}$, while the HVC is at $\sim 80 \text{ km s}^{-1}$.

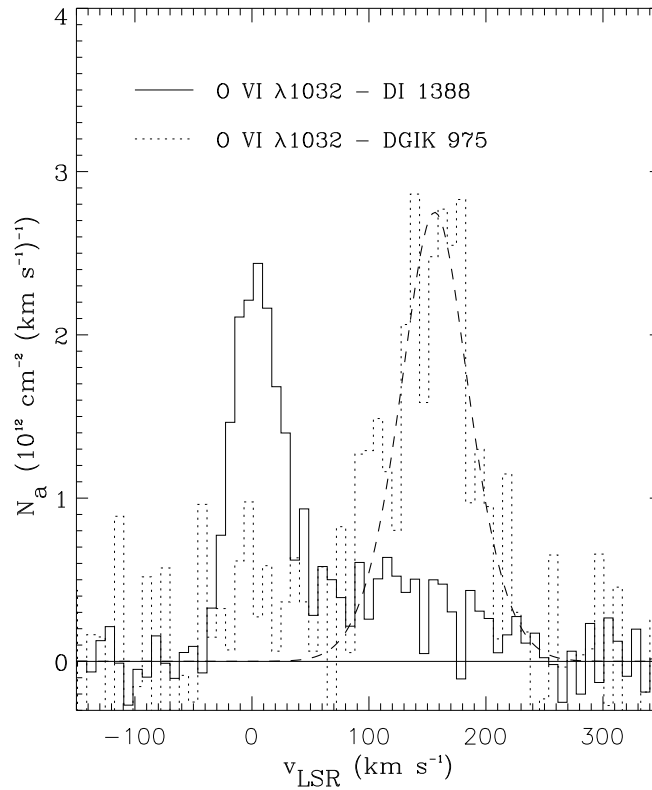


FIG. 11.— Comparison of the apparent column density profiles (*histograms*) for O VI in the direction of DI 1388 and DGIK 975. The dashed line is a Gaussian fit to the O VI absorption line.

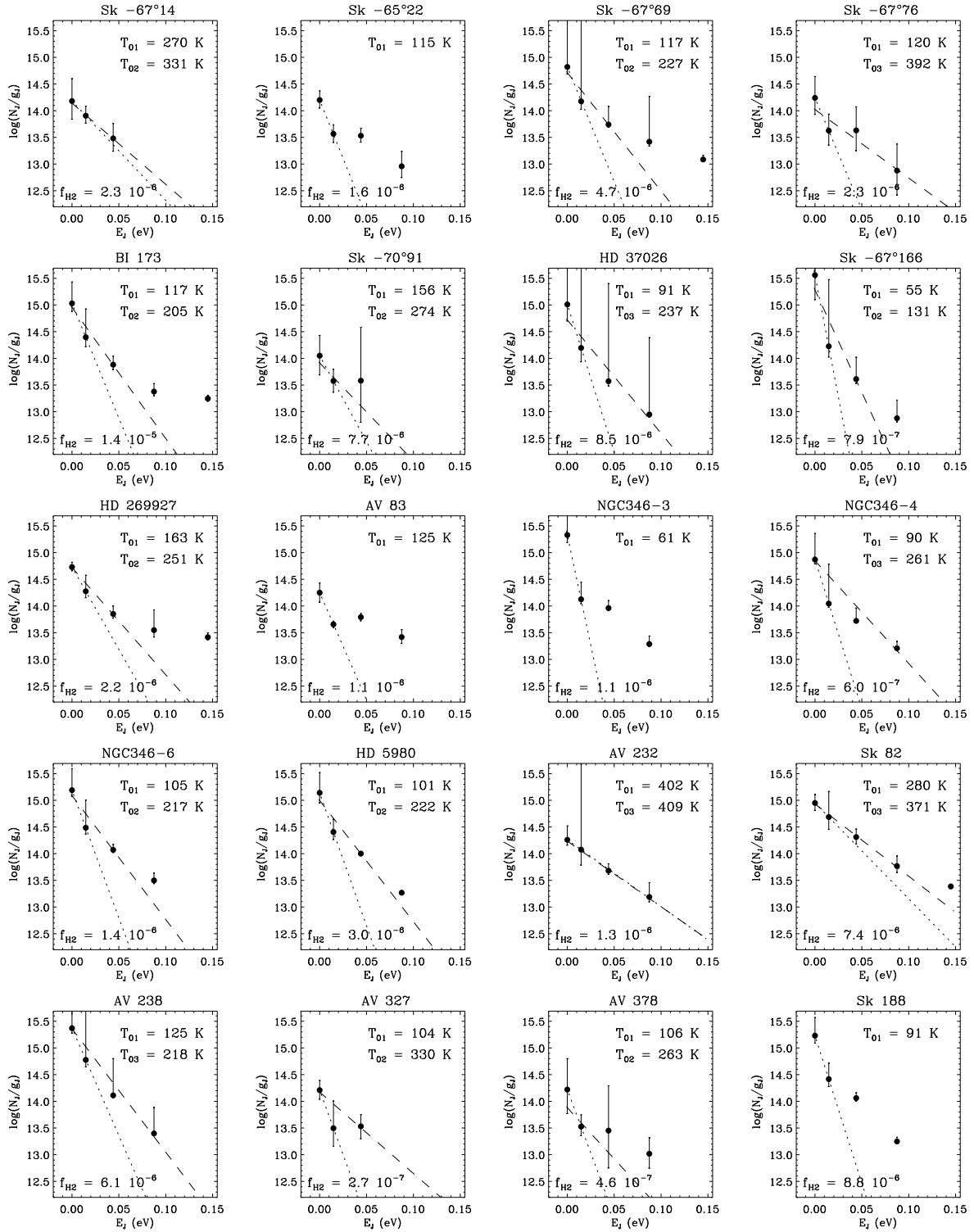


FIG. 12.— H_2 column density (N_J) divided by statistical weight (g_J) as a function of the excitation energy (E_J) for different rotational levels J in the LMC (first 9 panels) and the SMC. The $N(J)$ are from Tumlinson et al. (2002). The dotted line represents the excitation temperature T_{01} derived from Equation 1. When present, the dashed line is a least square fit to the $N(J)$ and T_{0j} (with $j > 1$), showing the resulting excitation temperature and j , the number of levels used (see Appendix for more details). In the left corner of each panel, the molecular fraction is indicated.